Remote Sensing of Environment 319 (2025) 114622

Contents lists available at ScienceDirect

Remote Sensing of Environment

journal homepage: www.elsevier.com/locate/rse

Cloud heights retrieval from passive satellite measurements using lapse rate information

Weiyuan Zhang [a], Jiming Li [a,b,*], Jiayi Li [a], Sihang Xu [a], Lijie Zhang [a], Yang Wang [a], Jianping Huang [a,b]

[a] College of Atmospheric Sciences, Lanzhou University, Lanzhou 730000, China
[b] Collaborative Innovation Center for Western Ecological Safety, Lanzhou University, Lanzhou 730000, China

ARTICLE INFO

Keywords:
Cloud height
passive satellite
lapse rate
CloudSat-CALIPSO
cloud geometrical thickness

ABSTRACT

Cloud top and base height (CTH and CBH) are essential in understanding the role of clouds on the weather and climate systems and improving radiation and precipitation simulations. However, inferring accurate cloud heights from passive satellite observations remains more challenging, especially for CBH. This study developed an effective and convenient method for estimating cloud heights for different cloud types on a global scale. The method is based on the mean lapse rate from surface to cloud top (Γ_{ct}), the lapse rate within (Γ_{cb1}) and below cloud (Γ_{cb2}), which are calculated from collocated active and passive satellite observations. The CTH and CBH can be easily derived based on cloud top temperature (CTT), surface temperature (ST), surface height (SH), Γ_{ct}, Γ_{cb1} and Γ_{cb2}. The lapse rate method was applied to polar-orbiting and geostationary passive satellites and the performances were evaluated using cloud heights measurements from CloudSat and CALIPSO satellite. Overall, our retrieval results can achieve high accuracy and stability in estimating both CTH and CBH. For example, our CTH results have significantly improved the retrieval accuracy, with mean bias error (MBE) is 0 km and R is 0.96, and the absolute bias error (MAE) and root mean square error (RMSE) are reduced from 1.12 km and 1.72 km to 0.85 km and 1.33 km, respectively, compared with the MODIS CTH product. Our CBH retrieval results based on MODIS CTT and ST also agree well with CloudSat and CALIPSO observations, the R is 0.91 and the MAE, MBE and RMSE are 0.73 km, 0 km and 1.26 km, respectively. The cloud geometric thickness derived from the cloud heights retrieval results also agrees well with the active satellite observations (MAE = 0.97 km, MBE = 0 km, RMSE = 1.44 km and $R = 0.91$). In addition, the good performance of cloud heights retrieval during night and for geostationary satellites can further illustrate the excellent accuracy and strong applicability of the lapse rate method. Specifically, compared with SatCORPS Himawari-8 product, the MAE and RMSE of CTH (CBH) are reduced by 41.5 % (44.2 %) and 39.4 % (36.6 %), respectively. These statistical results confirm that our method has comparable performance to other algorithms (e.g., machine learning and other empirical methods), in the meantime, exhibiting the advantages of simplicity and less input parameters. In addition, the lapse rate method can also be employed to provide a supplemental criterion on determining cloud layers from radiosonde data.

1. Introduction

Cloud heights, including cloud top height (CTH) and cloud base height (CBH), as important macroscopic parameters reflecting the cloud vertical distribution, have a very important impact on radiation balance and water cycle (Li et al., 2011; Simpson et al., 2000; Yan et al., 2016). For example, the radiative effects of clouds at different altitudes exhibit significant differences, low clouds typically reflect solar radiation resulting a cooling effect, whereas high cirrus clouds tend to warm the surface by preventing longwave radiation from emitting outward (Liou, 2002; Luo et al., 2023). Under the background of climate change, the increase in CTH also contributes to the positive longwave cloud feedback (Zelinka et al., 2012). Additionally, high CTH can serve as an indicator of deep convective precipitation in tropical regions (Biondi et al., 2013). Besides CTH, cloud base height is also the main factor in modulating the cloud radiation effects, especially for the downwelling radiation at the surface (Xu et al., 2021; Yeo et al., 2018). The breakup and coalescence of raindrops are related to the distance between the

* Corresponding author at: College of Atmospheric Sciences, Lanzhou University, Lanzhou 730000, China.
E-mail address: lijiming@lzu.edu.cn (J. Li).

https://doi.org/10.1016/j.rse.2025.114622
Received 23 August 2024; Received in revised form 5 January 2025; Accepted 26 January 2025
Available online 31 January 2025

cloud base and surface, thus CBH is also of great importance on precipitation characteristics (Adhikari et al., 2017). Moreover, accurate CBH knowledge is also crucial for aviation safety (Mecikalski et al., 2007). Therefore, deriving precise CTH and CBH information will significantly improve our understanding for the role of clouds in Earth's weather and climate change, as well as the simulations of radiation and precipitation in climate models (Cesana et al., 2019; Rajeevan and Nanjundiah, 2009; Viúdez-Mora et al., 2015).

Until now, the direct measurements of cloud height information can be obtained through ground-based instruments (e.g., lidar, cloud radar and ceilometer), but the limited spatial coverage prevents broader applications. Satellite remote sensing is the advanced method of obtaining cloud observations at global scales. Active space-borne instruments, such as Cloud Aerosol Lidar with Orthogonal Polarization (CALIOP) on the CALIPSO satellite and Cloud Profiling Radar (CPR) on the CloudSat satellite, can provide accurate cloud height measurements on a global scale (Winker et al., 2009). However, due to their narrow scanning swath, the observations are limited by restricted spatial coverage and longer revisit periods (Stephens et al., 2002). In contrast, passive satellites offer the advantage in providing long-term, large spatial coverage and high temporal resolution observations, which are vital for the development of high spatiotemporal resolution cloud height products. Therefore, developing accurate cloud heights retrieval algorithms based on passive satellite observations is very desired and valuable.

Over the past few decades, several algorithms for CTH retrieval have been developed, including infrared windows method, the split-window method, the CO_2-slicing method and oxygen A-band method (Heidinger and Pavolonis, 2009; Menzel et al., 2008; Rozanov and Kokhanovsky, 2004). Many passive sensors have provided operational CTH products, such as MODIS (Baum et al., 2012), the Advanced Himawari Imager (AHI) on board the Himawari-8 (H8) satellite (Iwabuchi et al., 2018) and the Advanced Geostationary Radiation Imager (AGRI) onboard Fengyun-4 A (Min et al., 2017). With the improvement of computational resources, some machine learning methods have been employed in estimating CTH for passive satellites. For instance, Min et al. (2020) and Yang et al. (2022) have achieved more accurate CTH retrieval using the gradient boosting decision tree (GBDT) and Extreme Gradient Boosting (XGBoost) models, respectively, compared to the operational H8 product. The potential of convolutional neural network in effective retrieval of CTH has also been demonstrated (Håkansson et al., 2018; Wang et al., 2022; Zhao et al., 2023b). In addition, lapse rate is also an important information to estimate CTH. Sun-Mack et al. (2014) proposed an approach for determining the low CTH using regional apparent boundary layer lapse rates derived from collocated CALIPSO and MODIS data.

Due to the inability of spectral signals to penetrate cloud layers, obtaining accurate CBH is more challenging. By using methods such as spectral matching or cloud type matching, CBH from active satellites can be extrapolated to a larger passive observation range (Barker et al., 2011; Miller et al., 2014; Sun et al., 2016). Another commonly used approach involves converting the cloud water path (CWP) into the cloud geometric thickness (CGT), and the CBH can be derived based on the difference between CTH and the CGT (Hutchison, 2002; Hutchison et al., 2006; Noh et al., 2017). Hutchison (2002) assumed that the relationship between CWP and CGT is primarily determined by cloud type, and used empirical cloud water content (CWC) for six cloud types. Noh et al. (2017) investigated the vertical variation of CWC, resulting in a more precise relationship between CWP and CGT. Tan et al. (2023) further considered the effects of more factors on the mean CWC, and the mean bias of retrieved CBH was reduced to 0.11 ± 1.93 km. Recently, the application of machine learning methods has also significantly improved the accuracy of CBH estimation. Tan et al. (2021) and Lin et al. (2022) developed CBH retrieval algorithms for single-layer clouds during daytime based on random forest and the Gradient Boosted Regression Trees (GBRT) models, respectively, and the retrieval results were in better agreement with active satellite observations. By using thermal infrared measurements, the all-day available algorithms based on random forest model (Shao et al., 2023) and convolutional neural network (Wang et al., 2023) have also been developed.

The above methods offer us numerous valuable references. However, due to the uncertainties of radiative transfer model in cloudy skies, the presence of temperature inversions, theoretical assumptions and so on (Hamann et al., 2014; McKee and Cox, 1976), there are still significant biases in these operational passive CTH products, especially for high and thin clouds (Baum et al., 2012; Huo et al., 2020b). The CTH derived from passive sensors tended to be lower than those from active satellites and ground-based radar (Huo et al., 2020b; Tan et al., 2019). In addition, the extrapolation method for CBH estimation is only applicable to relatively flat and uniform clouds, and is also limited by the extrapolation distance (Lu et al., 2021; Mülmenstädt et al., 2018). And the CWP-based method is not applicable during nighttime, as the CWP is generated based on solar channels. The machine learning methods do greatly improve the accuracy of the CTH and CBH retrieval. However, these algorithms typically necessitate the numerous spectral information and auxiliary meteorological field information as input, which may lead to limitations in the application of the algorithm to other passive satellites (Lin et al., 2022; Min et al., 2020).

Here, we apply the lapse rate information to estimate the CTH and CBH for passive satellites. This method is further improved based on our previous study (Li et al., 2013) and is expected to obtain more accurate cloud height information for different cloud types. The lapse rate method has the advantages of simplicity, fewer input parameters, high accuracy and wide applicability, and it can work both during day and at night. Thus, it may serve as a valuable supplement to currently available retrieval techniques based on passive sensors. This paper is organized as follows:The brief introduction of datasets used in this study is given in Section 2. Section 3 presents the theoretical description and construction of the lapse rate method used in the paper. Section 4 demonstrates the application of the method and analyses its performance. The conclusions and summary are presented in Section 5.

2. Data

2.1. MODIS data

The Moderate Resolution Imaging Spectroradiometer (MODIS) imager on the Aqua satellite was launched in 2002. This instrument can provide long-term observations on a global scale, with 36 spectral bands with wavelengths in the range of 0.4 μm to 14.4 μm. It includes almost all the important bands from visible to infrared (King et al., 2003; Platnick et al., 2003), and may cover the globe every one to two days with high spatial resolution from 250 m to 1 km (2 bands at 250 m, 5 bands at 500 m, and 29 bands at 1 km). In this study, the operational Aqua-MODIS Collection 6.1 Level 2 cloud products (MYD06_L2) were used. Specifically, parameters with a spatial resolution of 1 km, including surface temperature (ST), cloud top pressure (CTP), cloud top temperature (CTT), CTH and cloud optical thickness (COT) were used. The latest version of MODIS product uses the CO_2-slicing technique (Menzel et al., 2008) for CTP retrieval of mid- to high-level clouds, and the CTP is converted to CTH and CTT with the National Centers for Environmental Prediction Global Data Assimilation System (NCEP GDAS). For low clouds, however, the 11-μm infrared window technique is used to derive the CTH (Baum et al., 2012).

2.2. CloudSat and CALIPSO satellite data

Along with Aqua-MODIS, the CloudSat and CALIPSO satellites are both members of the A-train satellite constellation; the CloudSat satellite carries a 94GHz cloud profiling radar (CPR), and the CALIPSO satellite carries a two-wavelength Cloud–Aerosol Lidar with Orthogonal Polarization (CALIOP) (Stephens et al., 2008; Winker et al., 2009). The CPR can penetrate optically thick clouds that can attenuate lidar signals,

while lidar can detect optically thin clouds that are not detected by cloud radar. Thus, in this study, we used the 2B-GEOPROF-LIDAR dataset, which combines the advantages of CPR and CALIOP to accurately describe information on the vertical structure of clouds in the atmosphere on a global scale (Mace and Zhang, 2014; Mace et al., 2009). In this dataset, each profile consists of 125 height layers and can provide up to five layers of cloud boundary information. In the presence of multi-layered clouds, cloud properties retrieval from passive radiometers is highly uncertain (Naud et al., 2007; Teng et al., 2023). Therefore, following the previous studies (Lin et al., 2022; Tan et al., 2021), only the CBH and CTH of single-layer cloud samples identified by the 2B-GEOPROF-LIDAR product were used as the reference values to construct the method and validate the retrieval results.

2.3. Geostationary satellite data (H8 and GOES-13)

The method has also been extended to geostationary satellites. As the new-generation geostationary satellite, Himawari-8 was launched on 7 October 2014 and located at 140.7°E above the equator. The AHI on board H8 can capture information from 16 spectral channels, with the central wavelength ranging from 0.47 to 13.3 μm, including 3 visible, 3 near-infrared, and 10 thermal channels (Bessho et al., 2016). The Geostationary Operational Environmental Satellite-13 (GOES-13) launched on 24 May 2006, is a geostationary satellite operated by the National Oceanic and Atmospheric Administration (NOAA). It is located at 73°W above the equator, and the GOES N—P Imager aboard the satellite is a 5 channel (1 visible, 4 infrared) imaging radiometer. The Satellite Cloud and Radiation Property Retrieval System (SatCORPs) Clouds and the Earth's Radiant Energy System (CERES) Geostationary Satellite (GEO) Edition 4 dataset can provide hourly cloud physics and radiative properties of multiple geostationary satellites. In this study, the Himawari-8 and GOES-13 cloud products retrieved by SatCORPs algorithms supporting the CERES project were employed (Minnis et al., 2008). Similarly, the parameters including CTP, CTT, CTH, CBH and COT were extracted.

2.4. Other auxiliary datasets

As the geostationary satellite products employed in this study are unable to provide surface temperature for cloudy pixels, thus the surface temperature from ERA5 reanalysis was employed as a supplementary data source. ERA5 is the fifth-generation atmospheric reanalysis of the European Centre for Medium-Range Weather Forecasts (Hersbach et al., 2020). In this study, ERA5 hourly surface temperature with a horizontal resolution of 0.25° was used. The linear and inverse distance weighted interpolation algorithms were applied respectively to achieve temporal and spatial matching between ERA5 data and geostationary satellite observations. Table 1 summarizes the information of all the datasets used in this study and their corresponding parameters.

3. Methodology

3.1. Method description

The basic idea of our method is to use lapse rate information to estimate CTH and CBH based on passive satellites. The CTH retrieval requires calculating the mean lapse rate from the surface to the cloud top, defined as the ratio of the temperature difference to the height difference. In addition, the lapse rate within cloud (from cloud base to cloud top) and below cloud (from surface to cloud base) are needed for the CBH retrieval.

In order to ensure the accuracy of the lapse rate method, the first step is to understand the factors that influence the lapse rate. Previous studies have shown that using a fixed lapse rate to retrieve CTH is apparently not feasible everywhere (Dong et al., 2008), and the derived mean boundary lapse rate exhibits considerable spatial variability and pronounced seasonal fluctuations across most of the globe (Sun-Mack et al., 2014). There are also obvious regional differences in the lapse rates within and below the cloud (Li et al., 2013). Furthermore, the cloud type plays a crucial role in estimating CBH, and the algorithms usually exhibit enhanced performance when cloud type information is incorporated (Forsythe et al., 2000; Liang et al., 2017). Especially, using GPS Radio Occultation and CloudSat observations, Yang and Zou (2013, 2017) have indicated that the lapse rate within clouds depends on cloud types. Clouds can influence the atmospheric thermal states through latent heat release and radiative heating (Haynes et al., 2013). Different types of clouds have different physical properties. Factors such as cloud height, cloud optical thickness, cloud phase, cloud effective radius and cloud droplet concentration can affect the cloud radiation effects (Chen et al., 2000; Hartmann et al., 1992; Li et al., 2020; Zhao et al., 2023a), which also affect the temperature variations below and within the clouds, and hence the lapse rate. Also, different types of clouds are usually dominated by different physical processes (e.g., condensation growth, deposition and freezing). These processes can result in differences in the release of latent heat (Jakob and Schumacher, 2008), which further affects the lapse rate. In fact, due to the complexity and diversity of clouds in the real atmosphere, many other factors may also influence the lapse rates (e.g., atmospheric humidity and composition). Nevertheless, some variables cannot be observed in real time and splitting the samples too finely can result in an insufficient sample size and reduced stability of the method. As results, the effects of longitude, latitude, cloud type and season on the lapse rate were eventually accounted for when constructing the method.

For the CTH retrieval method, the mean temperature lapse rate from surface to cloud top (Γ_{ct}) can be defined as (Sun-Mack et al., 2014):

$$\Gamma_{ct} = \left(T_{suf} - T_{ct}\right) / \left(Z_{ct} - Z_{suf}\right) \quad (1)$$

where T_{ct} is the CTT derived from passive satellites, Z_{ct} and Z_{suf} are the CTH and surface elevation from active satellite, respectively. T_{suf} is surface temperature derived from passive satellite (for MODIS) or ERA5 reanalysis data (for geostationary satellites). In this study, it should be note that the mean lapse rate is derived from the cloud top and surface

Table 1
The details of datasets used in this study.

Products	Variables	Temporal Coverage	Spatial resolution	Temporal resolution	Functions
2B-GEOPROF-LIDAR	CTH; CBH; Cloud layer number; surface elevation	2007–2012, 2015–2017	1.4 × 1.7 km	Orbital Profiles	As target for method construction and validation
MYD06	ST; CTT; CTH; CTP; COT	2007–2010	1 km	Orbital View field	As input for method construction and validation
SatCORPS CERES GEO Edition 4	CTT; CTH; CTP; COT; CBH	2015–2017 for H8 and 2010–2012 for GOES-13	6 km for H8 and 8 km for GOES-13	1 h	As input for method construction and validation
ERA5	ST	2010–2012, 2015–2017	0.25°	1 h	As input for method construction and validation

temperatures, rather that the air temperatures at surface and cloud top in the standard definition of the lapse rate. Subsequently, the CTH can be calculated by means of the following equation:

$$Z_{ct} = 1/\Gamma_{ct}{}^{*}\left(T_{suf} - T_{ct}\right) + Z_{suf} \tag{2}$$

Furthermore, the temperature difference between the cloud top and surface ($T_{suf} - T_{ct}$) can be divided into two components. The first is the temperature difference between cloud top and base (within cloud), the other is the temperature variation between the cloud base and the ground (below cloud). As shown in the following equation (Li et al., 2013):

$$T_{suf} - T_{ct} = \Gamma_{cb1}\left(Z_{ct} - Z_{cb}\right) + \Gamma_{cb2}\left(Z_{cb} - Z_{suf}\right) \tag{3}$$

where Γ_{cb1} represents the lapse rate within cloud, and Γ_{cb2} is lapse rate below the cloud. Z_{cb} and Z_{ct} minus Z_{cb} are cloud base height and cloud geometric thickness derived from 2B-GEOPROF-LIDAR product. In order to retrieve the CBH, eq. (3) can be transformed as follows:

$$Z_{cb} - Z_{suf} = (1/\Gamma_{cb2})^{*}\left(T_{suf} - T_{ct}\right) - \left(\Gamma_{cb1}/\Gamma_{cb2}\right)^{*}\left(Z_{ct} - Z_{cb}\right) \tag{4}$$

The least squares fitting method allows the optimum estimates of the coefficients $a = 1/\Gamma_{cb2}$ and $b = -\Gamma_{cb1}/\Gamma_{cb2}$ to be obtained. The CBH can then be calculated using the following equation:

$$Z_{cb} = \left(a^{*}\left(T_{suf} - T_{ct}\right) + b^{*}Z_{ct} + Z_{suf}\right)/(1+b) \tag{5}$$

It should be noted that we also introduced residual term (ε) as a correction factor to improve the accuracy of our method. Firstly, for each training sample, the estimated CTH and CBH can be obtained using eqs. (2) and (5). The residuals represent the deviations between estimated cloud heights and active satellite observations in the training dataset. Furthermore, the CTH residual can be fitted as a function of ($T_{suf} - T_{ct}$), and the CBH deviations can be fitted as a function of CTH and ($T_{suf} - T_{ct}$). Then, we can obtain the fitting coefficients for CTH residual and CBH residual. Finally, the CTH and CBH can be inferred by following equations:

$$Z_{ct} = 1/\Gamma_{ct}{}^{*}\left(T_{suf} - T_{ct}\right) + Z_{suf} + \varepsilon\left(T_{suf} - T_{ct}\right) \tag{6}$$

$$Z_{cb} = \left(a^{*}\left(T_{suf} - T_{ct}\right) + b^{*}Z_{ct} + Z_{suf}\right)/(1+b) + \varepsilon\left(T_{suf} - T_{ct}, Z_{ct}\right) \tag{7}$$

After testing, we found that the residual term can improve the accuracy of our method. Consequently, for cloudy pixels, if the corresponding Γ_{ct} is known, the CTH can be calculated by T_{suf}, T_{ct} and Z_{suf} using eq. (6). And then the CBH can be calculated from the T_{suf}, T_{ct}, Z_{suf}, the retrieved CTH and the coefficients a and b, where a and b are related to the Γ_{cb1} and Γ_{cb2}.

3.2. Data processing

The flowchart of our data processing is shown in Fig.1. From the preceding theoretical description, it is apparent that the crucial point of the lapse rate method is to deduce the optimal values of lapse rates (including: Γ_{ct}, Γ_{cb1} and Γ_{cb2}). To develop the retrieval method for MODIS, four years (2007–2010) of MODIS and 2B-GEOPROF-LIDAR data were combined. And, the MODIS pixel closest to the CloudSat footprint within 1 km distance was selected. In addition, due to the high spatiotemporal variability of clouds, the time difference between the two observations was limited to 90 s.

After that, the cloud samples were randomly assigned into two groups, with 90 % used as the training dataset for method construction and 10 % as the validation dataset for evaluation of cloud heights

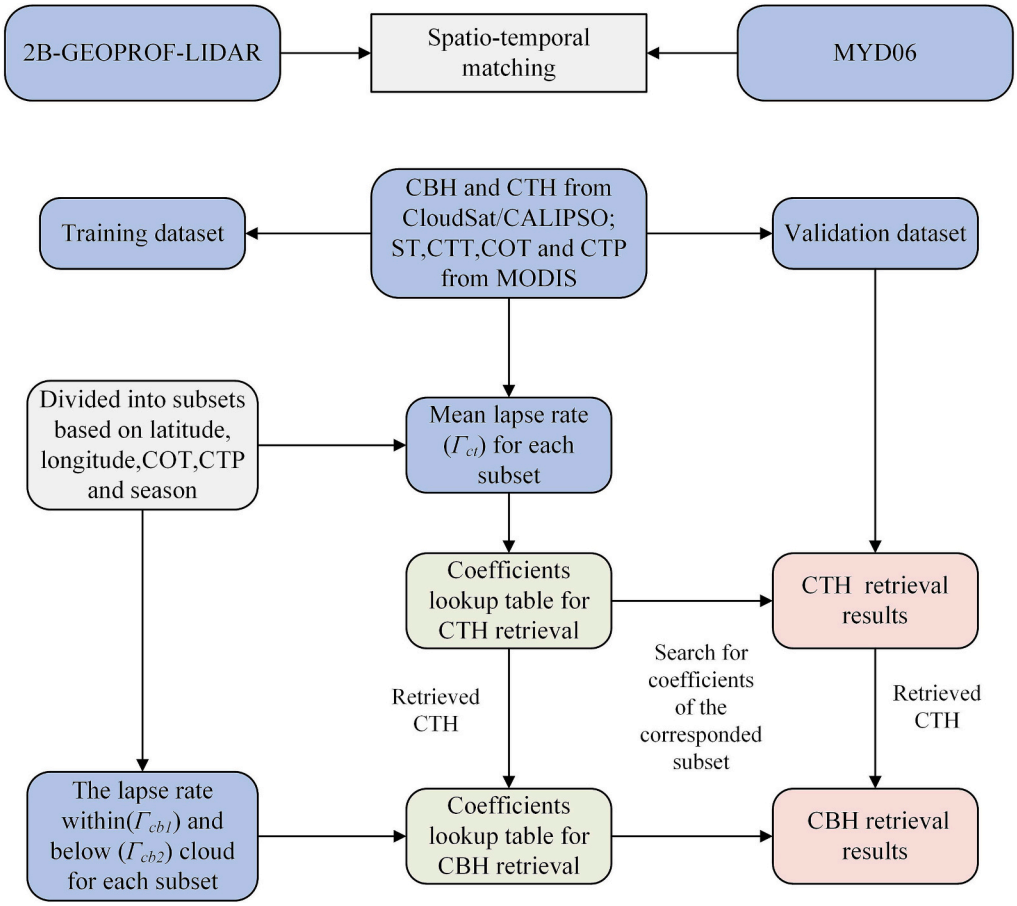

Fig. 1. The methodological workflow of our data processing section.

retrieval. Similar with Zhao et al. (2022), the cloud type classification is based on the joint distribution of cloud optical thickness (COT) and cloud top pressure (CTP). We therefore divided the samples in the training dataset into subsets (36 × 72 × 6 × 7 × 4) based on latitude, longitude, COT, CTP and season. Then, the samples in each subset were used to determine the representative coefficients. For CTH retrieval, we can obtain the Γ_{ct} for each collocated cloudy pixel using eq. (1). After testing, we found that the mean Γ_{ct} of all samples in each subset was more suitable as the representative Γ_{ct}. For CBH retrieval, the fittest values of coefficients a and b in each subset can be obtained by eq. (4) using least square method. Moreover, the fitted coefficients of the CTH and CBH residuals in each subset can be obtained, allowing the construction of the coefficient lookup tables for the cloud heights retrieval. Subsequently, for cloud heights retrieval of validation samples, CTH and CBH can be retrieved using eq. (6) and (7), with ST, CTT and coefficients for the given latitude, longitude, COT, CTP and season.

Fig. 2 shows the spatial distribution of three lapse rates coefficients (Γ_{ct}, Γ_{cb1} and Γ_{cb2}), as well as their joint histograms of CTP and COT. The Γ_{cb1} and Γ_{cb2} are calculated using the coefficients a ($1/\Gamma_{cb2}$) and b ($-\Gamma_{cb1}/\Gamma_{cb2}$). As in previous studies, the Γ_{ct} exhibits significant spatial variations, with values ranging from 1 to 11 K/km (Sun-Mack et al., 2014; Wu et al., 2008). The higher values were mainly located in typical stratocumulus regions and Tibetan Plateau region (Fig. 2a). Furthermore, there are significant differences in Γ_{ct} across different cloud types (Fig. 2d). Similarly, the lapse rate within (Γ_{cb1}) and below cloud (Γ_{cb2}) also have obvious spatial variations. For the Γ_{cb1}, larger values are observed at lower latitudes and smaller values at higher latitudes. However, for the Γ_{cb2}, which has smaller values at lower latitudes, with a minimum value of about 4 K/km. From 30° to the poles, it increases approximately with latitude. Moreover, both Γ_{cb1} and Γ_{cb2} vary somewhat between the various cloud types. As mentioned earlier, these differences can be attributed to variations in the cloud physical properties and different physical processes. The cloud heating rate and radiation fluxes are sensitive to changes in the cloud properties. Increasing the ice water content can result in an increase in longwave heating at cloud base and cooling near cloud top, and the liquid water content also alters the longwave hearting rate (Mather et al., 2007). In addition, differences in atmospheric temperature and water vapor profiles can lead to significant differences in cloud radiative effect (McFarlane et al., 2007; Yan et al., 2016). For lapse rate within cloud, our results are consistent with the observations of Yang and Zou (2013, 2017), with smaller values for low clouds, larger values for high clouds, and a slight increase with altitude. It is important to acknowledge that the lapse rates involved in this study represent only a statistical outcome and may not fully reflect the actual atmospheric environment. To summarize, all three lapse rates differ in spatial distribution and cloud type. Therefore, it is reasonable and necessary to consider the factors that may affect these lapse rates.

3.3. Evaluation metrics

Several error metrics were used to evaluate the performance of our method, including: mean absolute bias error (MAE), mean bias error (MBE), root mean square error (RMSE) and Pearson correlation coefficient (R). They are calculated as follows:

$$MAE = \frac{1}{n}\sum_{i=1}^{n}|y_i - x_i| \tag{8}$$

$$MBE = \frac{1}{n}\sum_{i=1}^{n}(y_i - x_i) \tag{9}$$

$$RMSE = \sqrt{\frac{1}{n}\sum_{i=1}^{n}(y_i - x_i)^2} \tag{10}$$

$$R = \frac{\sum_{i=1}^{n}(y_i - \overline{y})(x_i - \overline{x})}{\sqrt{\sum_{i=1}^{n}(x_i - \overline{x})^2 \sum_{i=1}^{n}(y_i - \overline{y})^2}} \tag{11}$$

in which n is the sample number, y_i is ith retrieval result, x_i is ith observation value. The $\overline{y}$ and $\overline{x}$ are the mean value of retrieval results and observations, respectively. Among them, a higher R, a lower MAE and RMSE, and a closer MBE is to 0 indicate better agreement between retrieved and observed results with less error.

4. Results

4.1. Overall performance of the method based on MODIS

We initially applied our cloud top and base height retrieval methods to the CPR-CALIOP-MODIS collocated validation dataset for method performance testing. The retrieval results were evaluated using CloudSat-CALIPSO product.

Fig. 3 shows the comparisons of CTH derived from MODIS product and new method (that is, lapse rate method) with CloudSat-CALIPSO

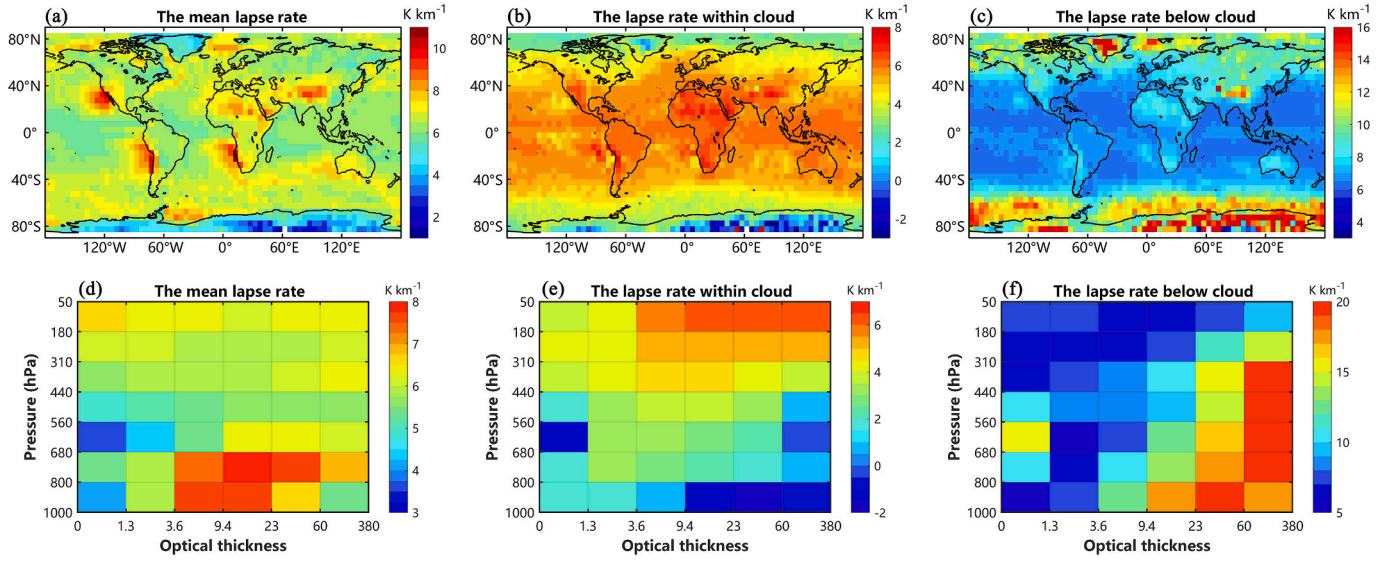

Fig. 2. Geographical distribution of (a) the mean lapse rate (Γ_{ct}), (b) the lapse rate within (Γ_{cb1}) and (c) below clouds (Γ_{cb2}). (d-f) are their joint histograms of cloud top pressure and cloud optical thickness.

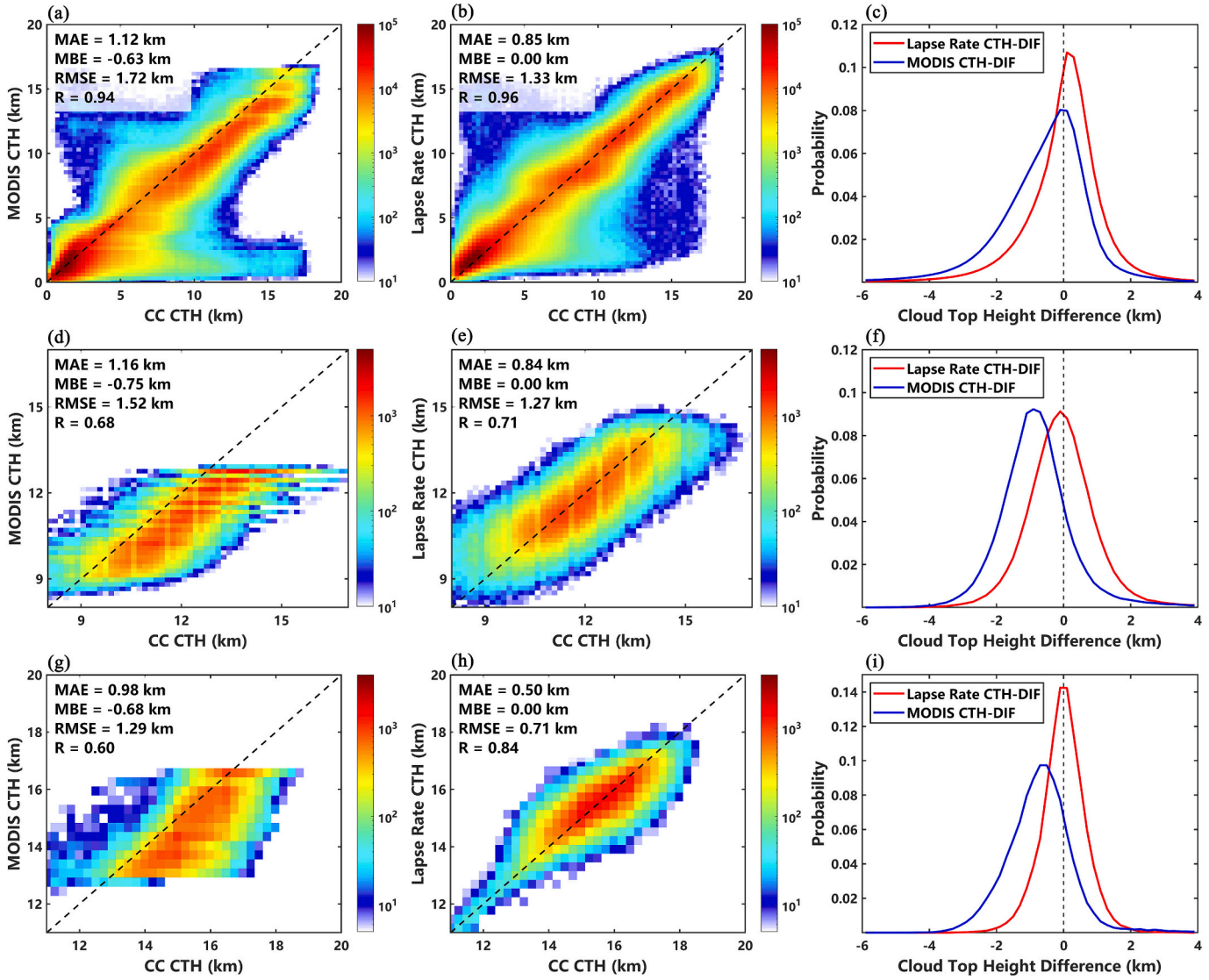

Fig. 3. Pixel-by-pixel comparisons of (a) MODIS CTH, and (b) our CTH retrieval results with CloudSat-CALIPSO measurements for all validation dataset samples at daytime. The colors indicate the number of samples. (c) The probability distribution of CTH differences between CC measurements and MODIS product (blue line), and our retrieval results (red line). Positive (negative) values indicate that a given dataset provides larger (smaller) CTH values than those of CC. The second row (d-f) is same as first row but for cloud samples with 1.3 < COT<3.6 and 180 hPa < CTP < 310 hPa, and the third row (g-i) is the result for cloud samples with 60 < COT<380 and 50 hPa < CTP < 180 hPa. (For interpretation of the references to colour in this figure legend, the reader is referred to the web version of this article.)

(hereafter, CC) measurements at daytime. And the corresponding evaluation metrics are also provided in the upper left corner of the relevant subplot. The density scatter plots of CC compared with MODIS and lapse rate method are shown in the first and second columns, respectively. It can be found that for all validation samples without regard to cloud types, the MAE of MODIS is 1.12 km, the MBE is −0.63 km, and the RMSE and R are 1.72 km and 0.94, respectively (Fig. 3a). In general, the MODIS underestimated CTH, particularly for samples with CTH exceeding 10 km, which is similar with previous studies (Min et al., 2020; Zhang et al., 2020), and the underestimation of CTH is primarily attributable to the limitations of passive sensors in detecting high optically thin clouds (Baum et al., 2012; Holz et al., 2008; Weisz et al., 2007). Fig. 3b indicates that our retrieval results exhibit a better consistency with the CC observations, with more samples clustered around the 1:1 line. The MAE, MBE, RMSE, and R values are superior to those of MODIS product, with values of 0.85 km, 0 km, 1.33 km and 0.96, respectively. Our lapse rate method effectively mitigates the MODIS underestimation in CTH, with an MBE improvement of 0.63 km. Our retrieval results also have comparable accuracy to the results of Håkansson et al. (2018), who developed a neural network approach for CTH retrieval from MODIS, and the MAE and RMSE of their results for all cloud samples are 0.98 km and 1.84 km, respectively. The probability distribution of the CTH deviation also indicates that our method is more accurate in estimating CTH, with the probability of deviation within ±1 km improved from 61 % to 72 % (Fig. 3c). It is worth noting that there are some samples with significant overestimation or underestimation in both the MODIS CTH product (Fig. 3a) and our retrieval results (Fig. 3b). The uncertainty in the spatiotemporal match of different sensors may result in large errors in MODIS CTH products. Large MODIS CTH deviations means large CTT deviations, resulting in the bias for the above samples remaining relatively large in our results.

Here, we also further evaluate the performance of our method for different cloud types. As a sample, the validations for high optically thin clouds (1.3 < COT<3.6 and 180 hPa < CTP < 310 hPa) and high optically thick clouds (60 < COT<380 and 50 hPa < CTP < 180 hPa) are shown in Fig. 3d-f and Fig. 3g-i, respectively. It is crucial to highlight that cloud types were classified according to the physical characteristics from MODIS product. There are significant underestimations of MODIS

for both types of samples, particularly in the case of high optically thin clouds, with MBE of −0.75 km and R of 0.68. When using the lapse rate method, we find significant improvements in MAE, MBE, RMSE, and R for both types of samples. For high optically thick (thin) clouds, the MAE and RMSE are reduced 0.48 km (0.32 km) and 0.58 km (0.25 km). The distribution of deviations also suggests that our method effectively mitigates the CTH underestimation, with the probability peak occurring near 0 km, and the MBE values are all 0 km. In summary, the CTH obtained by the lapse rate method is in good agreement with those of CC observations, with small MAE, RMSE and large R, indicating that the lapse rate method is more accurate and stable compared with MODIS CTH product.

Furthermore, we also evaluated the accuracy of the CBH retrieval based on our method. Due to the lack of the operational cloud base height product from MODIS, only the comparisons of the retrieved CBH with the CC observations are shown in Fig. 4. The first row presents the overall results for complete samples, while the second and third rows present the results for two specific cloud types. Fig. 4a demonstrates that the lapse rate method generally performs well in CBH estimation, and the most of samples are around the 1:1 line. The values of MAE, MBE, RMSE and R are 0.73 km, 0 km, 1.26 km and 0.91, respectively. In comparison, Tan et al. (2023) developed a CBH retrieval method by introducing the effective CWC variable. According to their results for MODIS single-layer non-precipitation clouds, the MBE is 0.11 km and R is 0.87. Wang et al. (2023) developed a deep learning model to estimate MODIS CBH using six thermal infrared radiances, COT, CTH, land cover,

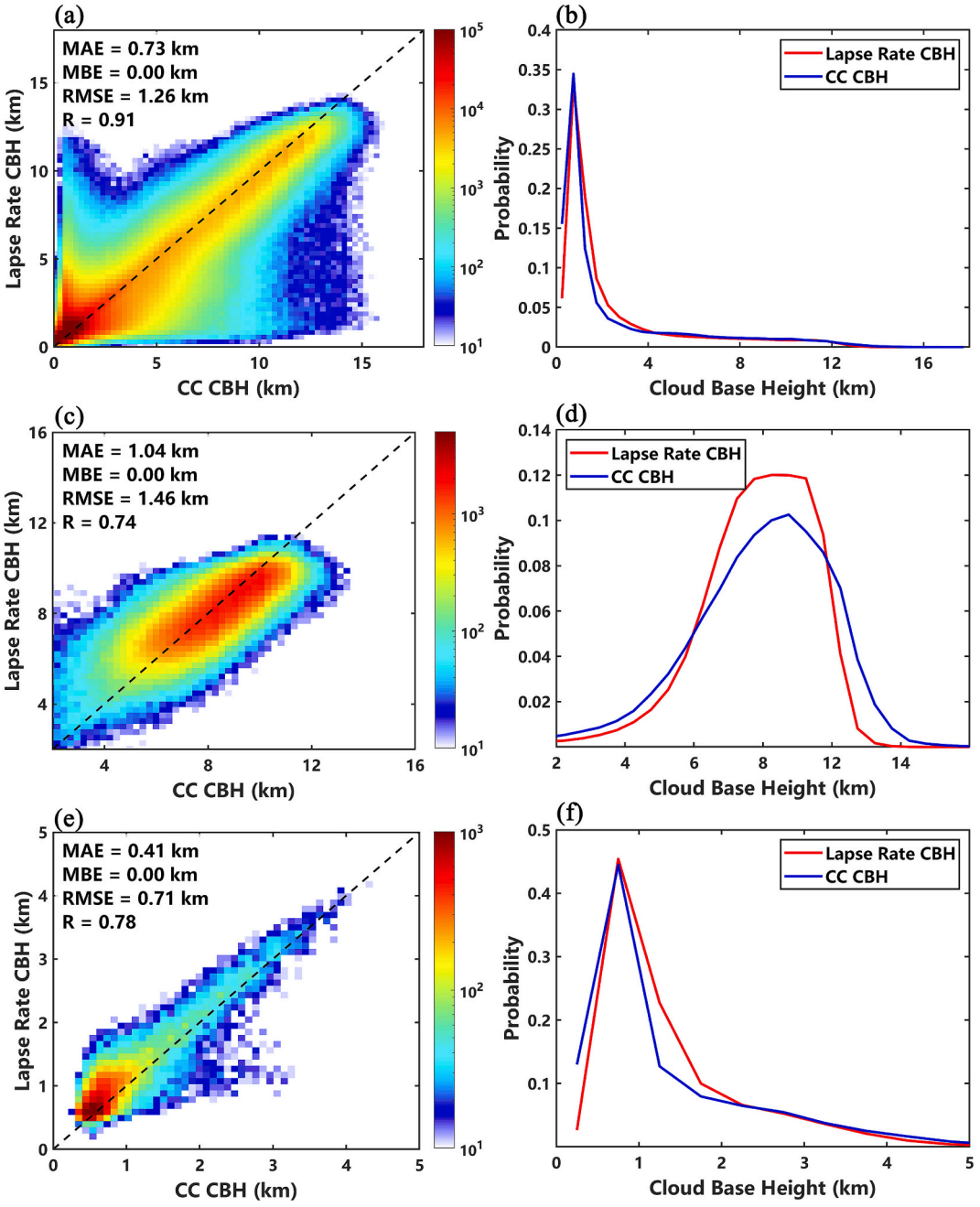

Fig. 4. Comparisons of CBH retrieval results with CC measurements at daytime. (a) Density scatter plot for all validation samples. (b) The probability distribution of CC CBH (blue line) and retrieved CBH (red line). The second row (c-d) is same as first row but for high optically thin clouds (1.3 < COT<3.6, 180 hPa < CTP < 310 hPa). The third row (e-f) is the result of cloud samples with 60 < COT<380 and 440 hPa < CTP < 560 hPa. (For interpretation of the references to colour in this figure legend, the reader is referred to the web version of this article.)

altitude and lifting condensation level, and the MBE, RMSE and R of their results for single-layer clouds are −0.22 km, 1.19 km and 0.94, respectively. This shows that the lapse rate method using only a few variables exhibits comparable performance compared to other algorithms. The negligible differences in the CBH probability distribution between CC products and our retrieved results can further demonstrate the excellent performance (Fig. 4b).

As a sample, the lapse rate method also performs well for high optically thin clouds (1.3 < COT<3.6, 180 hPa < CTP < 310 hPa), the CBH estimations agree well with CC observations, with R of 0.74 and MBE of 0 km (Fig. 4c). The probability distribution of our results and CC observations are similar (Fig. 4d). For cloud samples with 60 < COT<380 and 440 hPa < CTP < 560 hPa, the MAE and RMSE of retrieved CBH are 0.41 km and 0.71 km, respectively (Fig. 4e). The probability distribution is shown in Fig. 4f, it can be found that our results slightly overestimate the probability of CBH occurring in the 1–2 km range. Overall, the lapse rate method has high accuracy and stability, and provides good performance for all samples and two specific types of samples.

The lapse rate method is also available during nighttime. It should be noted that the MODIS COT product is generated based on solar channel information, and is not available at night. Consequently, different from the daytime case, the nighttime samples were divided into 36× 72 × 7 × 4 subsets based on latitude, longitude, CTP, and season. Thereafter, the most appropriate coefficients were obtained for each subset, which were then employed to retrieve the cloud top and base height. And the retrieval results during nighttime in 2007 is shown in Fig. 5.

Similarly, MODIS tends to underestimate CTH, especially for high clouds (Fig. 5a). The values of MBE and RMSE are −1.03 km and 2.63 km, respectively. The lapse rate method also performs well in estimating CTH at night, and the results agree better with observations. All four statistical metrics have improved, with MAE, MBE, RMSE and R values of 1.13 km, 0 km, 1.82 km and 0.92, respectively (Fig. 5b). As illustrated in Fig. 5c, the probability of the deviation being within ±1 km increased from 54 % to 64 %, and our method effectively alleviates the underestimation of MODIS CTH. The retrieved CBH also agrees well with the CC product, despite a certain degree of bias (MAE = 1.21 km and RMSE = 2.00 km). Furthermore, the probability distribution of estimated CBH is also in good agreement with observations (Fig. 5e).

It's worth noting that the CBH measurements of CC may be affected by surface clutter and precipitation. Previous studies have shown that CC has difficulty in detecting CBH of low clouds due to surface clutter, and underestimates cloud occurrence at lower altitudes (Bertrand et al., 2024; Cho et al., 2015). In addition, radar echo signal of precipitation can cause CPR to report a lower CBH than the "true" CBH (Noh et al., 2017). As only CC product are currently suitable as reference values, this may cause some bias in our results. Here, the collocated CloudSat-MODIS samples were further matched with the ground-based observations at SGP site, and CBH comparison results are shown in Fig. S1. The precipitation flag from the 2C-PRECIP-COLUMN product was used to identify precipitation. For the non-precipitation case, it can be found that due to ground clutter, CC may overestimate the near-surface CBH, and further overestimate probability within 1–2 km (Fig. S1a-b). Since our method used CC CBH as reference values, it shows similar biases to the CC CBH below 2 km. Above 2 km, CC agrees better than our results with ground-based observations (Fig. S1c-d). For the precipitation case, precipitation causes CC to underestimate the high level CBH, and CC CBH are all concentrated near 1 km, thereby significantly underestimating the probability within 2–5 km and overestimating the probability within 0.75–1.25 km (Fig. S1e-f). Compared to CC, our results alleviate the significant CBH underestimation. The scatter plot also shows our results are more consistent with the ground-based observations, with less bias (Fig. S1g-h).

Here, our CBH results in Fig.4–5 contain both precipitation and non-precipitation cloud samples. Although the overall MBE of our results is 0 km, there is an overestimation for low cloud bases. As we mentioned above, this overestimation is largely due to the anomalously low CC CBH of precipitation samples. Fig. S2 shows that for precipitation samples in

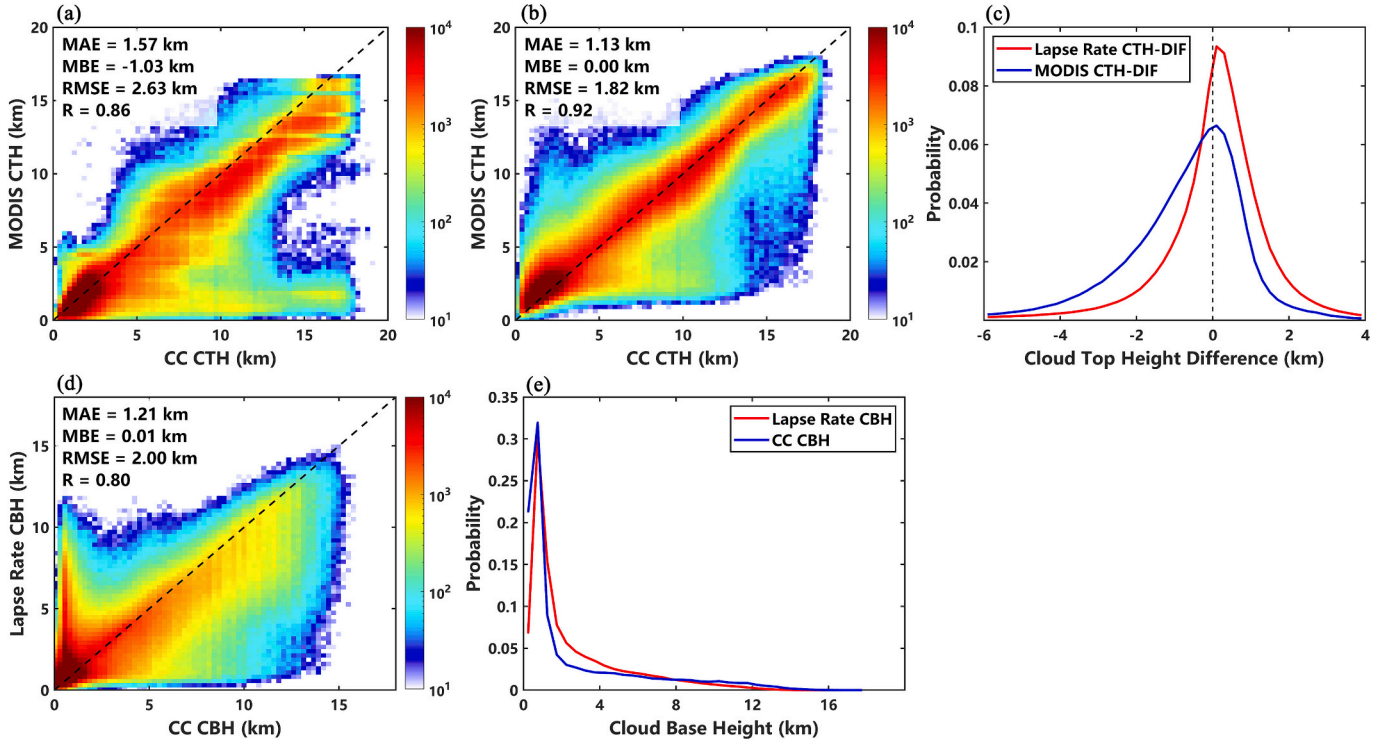

Fig. 5. The method validations of (a) MODIS CTH, (b) retrieved CTH and (d) retrieved CBH at nighttime. (c) is the probability distribution of CTH differences between CC measurements and MODIS product (blue line), and our results (red line). (e) is probability distribution of CBH. (For interpretation of the references to colour in this figure legend, the reader is referred to the web version of this article.)

Fig.4a, our CBH results are usually larger than those from CC (MBE = 0.54 km). For non-precipitation samples in Fig.4a, the overestimation for low cloud base is significantly alleviated (Fig.S2c). Moreover, the bias in MODIS CTT may also contribute to the overestimation of CBH. It is worth noting that the CC CBH of precipitation samples is anomalously low, which means that our results may be closer to the "true" values.

In addition, when we filter out precipitation samples from both the training and validation sets, the CBH retrieval results are shown in Fig. S3. It can be found that both the underestimation and overestimation for low cloud base heights in our results are significantly alleviated. Especially, the retrieved CBH are more consistent with the observations at night, with MAE reducing to 1.16 km and R improving to 0.86. During daytime, we have classified samples using COT and CTP, which improved the retrieval accuracy. This may also cause our accuracy to be less sensitive to precipitation removal. Previous studies have shown that COT is crucial in estimating CBH (Lin et al., 2022; Noh et al., 2017; Tan et al., 2021). The absence of MODIS COT during nighttime prevents the data from being divided according to COT and obtaining corresponding lapse rate, which has reduced the accuracy of CBH retrieval at night. Therefore, high-precision nighttime cloud optical thickness product for passive satellites would contribute to better performance of our lapse rate method.

The CGT is also a very important macro-physical property, and it affects the probability and intensity of precipitation, as well as liquid size and precipitation rate (King et al., 2015; Yan et al., 2016). The CGT estimation can be derived from retrieved CTH and CBH, and its comparison with CC is shown in Fig. 6. The estimated CGT also agrees well with observations (R = 0.91). The overall deviation is also relatively small, with MAE and RMSE of 0.97 km and 1.44 km, respectively. Tan et al. (2023) also obtained the CGT estimations for MODIS using an effective CWC lookup table, with MBE and R values of −0.36 km and 0.83, respectively. Yang and Cheng (2020) used a regression model to calculate CGT based on COT, cloud effective radius, and CTT. Their model performed best on the ocean, with the RMSE and R^2 of 1.74 km and 0.7. Using Orbiting Carbon Observatory-2(OCO-2) hyper-spectral oxygen A-band (O2A) observations, Li and Yang (2024) developed a CGT retrieving method for single layer liquid clouds, achieving R and MBE values of 0.78 and − 0.16 km for marine clouds after removing outliers. Compared with other methods, our CGT results show a certain improvement in accuracy, nevertheless, the distributions of CGT derived from lapse rate method and CC observations also indicate that our results underestimate the probability of CGT in the range of 0–500 m and overestimate the probability in the range of 500–1500 m (Fig. 6b). Our CGT results are based on CTH and CBH retrievals, and we find that the overestimation of CTH retrievals is the main reason for the above phenomenon. For some samples with observed CGT between 0 and 500 m, we have overestimated their CGT to be between 500 and 1500 m.

In addition, we have also extended the derived lapse rate to daytime cloud heights retrieval for MODIS in 2016, and the validation of our retrieval results is shown in Fig. S4. It can be found that the retrieval results of the CTH, CBH and CGT are also in good agreement with the CC product. Furthermore, the accuracy all remains consistent with previous results, which demonstrates the versatility and credibility of our method.

4.2. *Specific performance of the method during the daytime*

The absence of MODIS nighttime COT affects the accuracy of our method. Therefore, in this section, only daytime samples were selected to analyze the specific method performance for different seasons, regions and cloud types. The validation results for CTH and CBH in each season are shown in Fig. 7. Our lapse rate method performs well in both CBH and CTH estimation throughout the year, with strong stability across different seasons. Compared with the MODIS CTH product, the CTH retrieval results based on the lapse rate method demonstrate greater consistency with observations across all four seasons, exhibiting smaller errors and larger correlation coefficients. In particular, the negative bias of MODIS CTH (MBE <0 km) is significantly alleviated, and the MBE of the retrieved CTH is almost always 0 km (Fig. 7b). The retrieved CBH is also in good agreement with observations and has robust stability, with R exceeding 0.9 and MAE below 0.8 km in all four seasons. The MBE of retrieved CTH and CBH are very close to 0 km, resulting in their almost non-display on the Fig. 7b.

Fig. 8 shows the spatial performance of the MODIS CTH product, and the lapse rate method in estimating CTH and CBH. At first glance, the global MAE and RMSE distributions all have similar distribution patterns. The deviation of MODIS CTH is relatively larger in the equatorial regions, where high clouds are frequent existed. The ascending branch of the Hadley circulation can transport abundant water vapor to high altitudes, resulting in the formation of high clouds (Chi et al., 2024), and MODIS generally underestimates the CTH of these high clouds. The MODIS product uses a combination of the CO_2-slicing technique and the 11-μm infrared window (IRW) technique to retrieve CTH (Baum et al., 2012). The CO_2-slicing technique uses the measured radiance and clear-sky radiance from two neighboring wavelengths to derive CTP, and then CTH and CTT is derived from atmospheric profile data. The IRW method assumes that clouds are black bodies, and the measured 11-μm infrared brightness temperature is used to derive CTH by comparing with the brightness temperature profile derived from the NCEP GDAS (Baum et al., 2012). The uncertainty in theoretical assumption, atmospheric

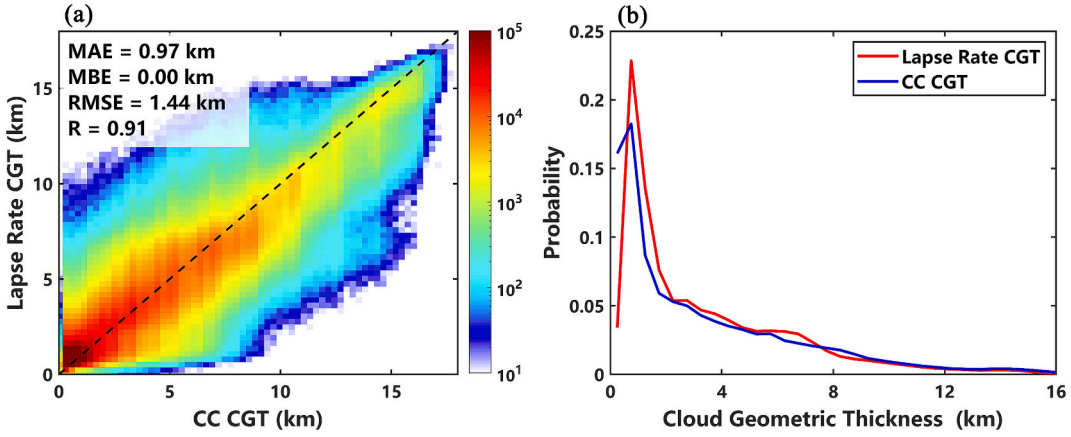

Fig. 6. Comparisons of CGT derived from lapse rate method with CC measurements at daytime. (a) Density scatter plot for all validation dataset samples, and (b) The probability distribution of CGT from CC measurements (blue line) and lapse rate method (red line). (For interpretation of the references to colour in this figure legend, the reader is referred to the web version of this article.)

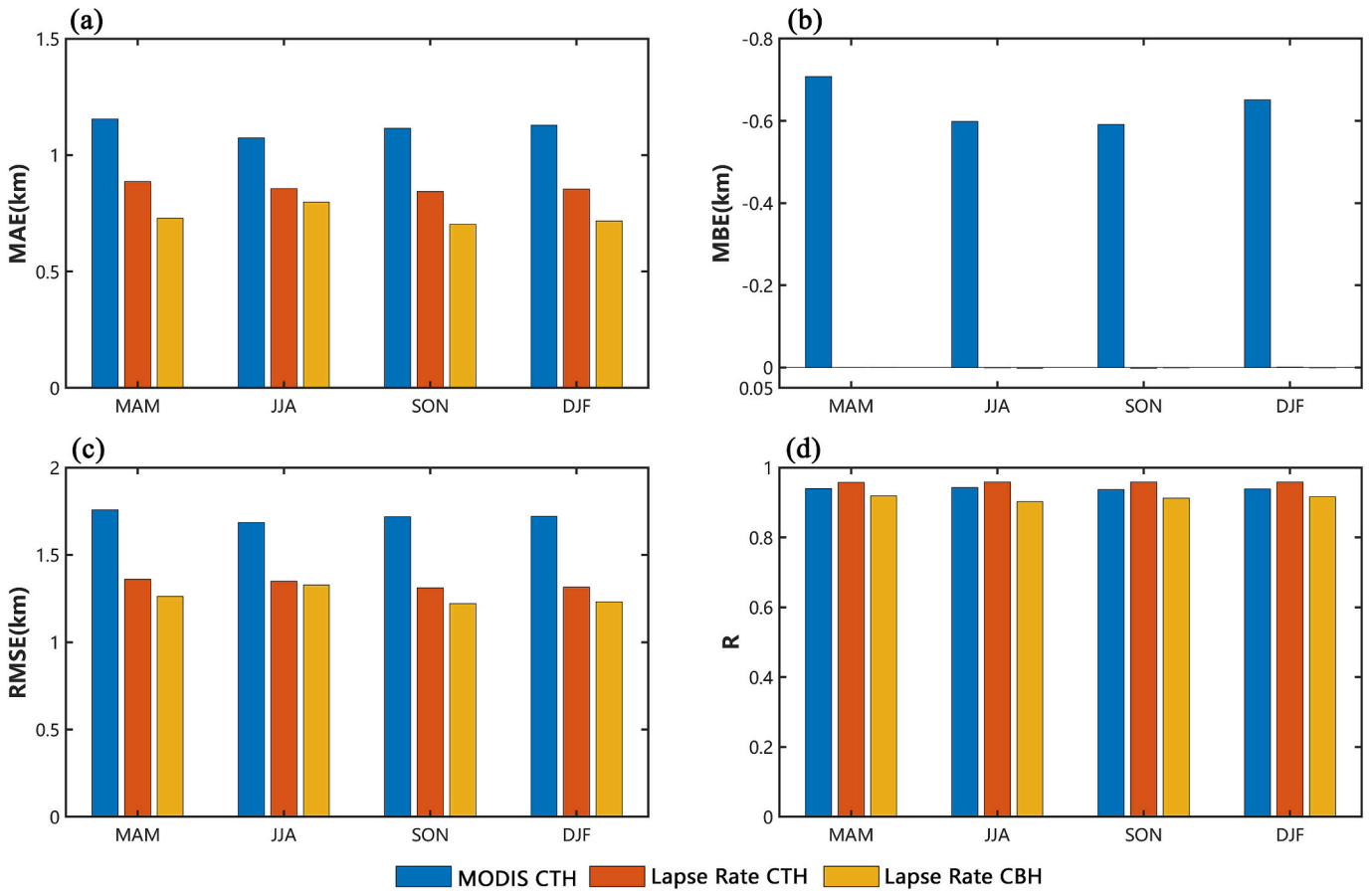

Fig. 7. Assessment of MODIS CTH product, retrieved CTH and retrieved CBH across different seasons. (a), (b), (c) and (d) are MAE, MBE, RMSE and R, respectively. The MBE of retrieved CTH and CBH are very close to 0 km, resulting in their almost non-display on the Fig. 7b.

temperature profile and radiative transfer model may affect the accuracy of CTT and CTH retrieval (Menzel et al., 2008). For the MODIS product, samples with a large CTH bias means a large CTT bias. Since the CTT is required to retrieve cloud heights, the errors in the CTT will be propagated into the CTH and CBH retrievals. In the typical stratocumulus cloud regions, both MAE and RMSE are relatively small, with MAE typically being less than 0.7 km. In addition, MODIS exhibits smaller CTH than radar-lidar measurements in most areas (MBE <0 km) except several stratocumulus cloud regions.

The statistical metrics of retrieved CTH have similar spatial distribution patterns to that of MODIS CTH, however, the specific values of the deviations have been reduced globally. According to Fig. 8d-e, the MAE and RMSE of retrieved CTH from our method have both decreased significantly, with the mean values reduced from 1.1 km and 1.7 km to 0.8 km and 1.3 km, respectively. Differences of statistical metrics between different regions have also been reduced, indicating a more stable spatial performance of the lapse rate method. The underestimation in CTH is also significantly alleviated (Fig. 8f), with the mean value of MBE is 0 km. The results of the CBH retrieved by lapse rate method are comparable to those reported by Wang et al. (2023), who developed a deep learning algorithm using thermal infrared radiances, cloud properties, land cover, altitude and lifting condensation level. Fig. 8g-i shows that the errors of retrieved CBH are relatively larger in the Intertropical Convergence Zone (ITCZ), where high optically thin clouds often occur. For those thin clouds, MODIS significantly overestimates the CTT (Holz et al., 2008). In most of the other regions, the deviations of the CBH estimations are small, especially in the subtropical stratocumulus region. Furthermore, the MBE is nearly 0 km on a global scale. In conclusion, the above results demonstrate that the lapse rate method has relatively high accuracy and stability in both CTH and CBH retrieval at the global scale, and the retrieved CTH is more accurate compared with MODIS CTH product. The corresponding number of validation samples for each grid is shown in Fig. S5. It can be found that there is no clear correspondence between the performance of our method and sample size, indicating that the better performance of our method is not due to more samples.

Furthermore, we also evaluated the performance of the lapse rate method on different cloud types. The MAE, RMSE and MBE for 42 cloud regimes sorted by CTP and COT are shown in Fig. 9. The distribution patterns of MAE and RMSE for MODIS CTH product are basically the same. In general, the deviation is smaller for middle and low clouds with larger optical thicknesses. It is evident that MODIS has large deviations for cloud samples with high CTP (CTP $>$ 440 hPa) and low COT (COT$<$3.6), and the largest MAE and RMSE can reach 4.89 km and 5.59 km, respectively (Fig. 9a-b). Combined with the corresponding negative MBE values, it suggests that the MODIS severely underestimates the CTH for these cloud types. For example, the samples identified by active satellite as high clouds may be misjudged by MODIS as lower clouds. This is due to that both the IRW method and CO_2-slicing method tends to determine CTH from the radiation center of the cloud layer, which might be lower than the actual cloud top (Huo et al., 2020a). For optically thin clouds, the difference between cloud radiance and clear-sky radiance is small, and the assumption that clouds are black bodies may not be true. Moreover, the longwave radiation emitted from the ground can penetrate clouds and affect satellite radiation measurements (Sassen and Campbell, 2001). All of these can lead to deviations in MODIS CTH. In addition, 41 of the 42 cloud types exhibit negative MBE (Fig. 9c), which also indicates that the MODIS underestimation of CTH is widespread. In comparison, the statistical metrics of retrieved CTH based on lapse rate method have similar distributions to those of MODIS, but the specific

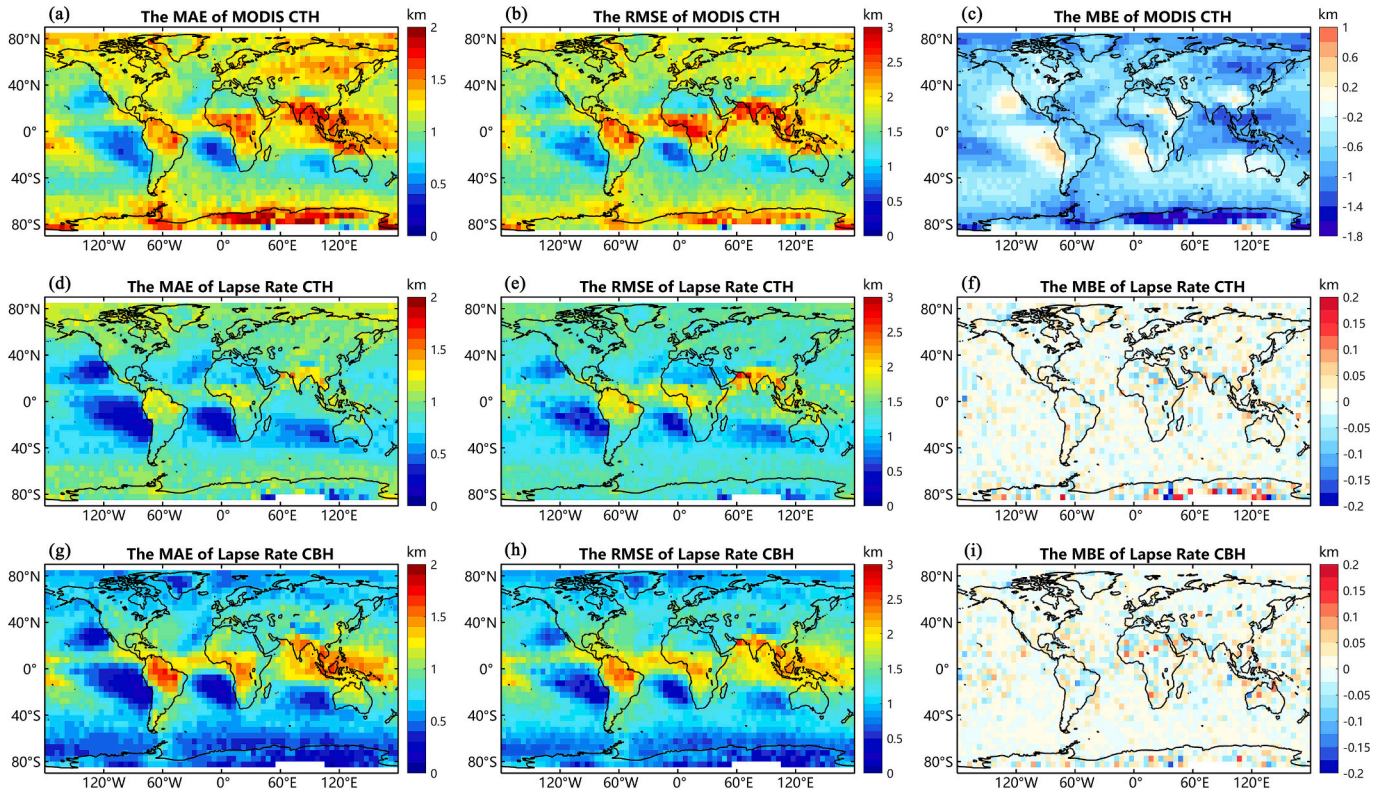

Fig. 8. Global distributions of MAE (a, d, g), RMSE (b, e, h), and MBE (c, f, i) in 5° × 5° grids. The first row is the results of MODIS CTH product, the second row is the results of CTH retrieval, and the third row is the results of CBH retrieval.

values are much improved (Fig. 9d-f). The maximum values of MAE, RMSE are reduced to 2.03 km and 2.75 km, respectively. A total of 30 types of samples exhibited an MAE of less than 1 km, while MODIS only has 9 types. The RMSE for 34 types of samples is less than 1.5 km (only 16 types for MODIS), and MBE values for all cloud types are nearly 0 km, significantly mitigating the underestimation of MODIS CTH. It is noteworthy that the MAE and RMSE of the retrieved CTH are significantly reduced for each cloud type when compared to the MODIS product.

According to Fig. 9g-i, the retrieved CBH from lapse rate method exhibits a good consistency with active observations, with MAE of 27 cloud types less than 1 km and most MBE values are very close to 0 km. The errors for middle and low optically thick clouds are the smallest, with MAE less than 0.5 km. The deviation of CBH is relatively larger for the samples misidentified by MODIS as low optically thin clouds. The deviations in MODIS CTT (CTH) can lead to deviations in the retrieved CTH, and then the deviations of MODIS CTT and retrieved CTH would affect the CBH retrieval. Through the above analysis, it can be found that the lapse rate method also has relative better performance in both CTH and CBH retrieval for different cloud types.

A suitable typhoon event has also been selected to demonstrate the concrete performance of our method. Fig. 10 shows across-section comparison results during the Hurricane Igor. The gray shading represents cloud layers derived from the joint CloudSat and CALIPSO product, and the results from MODIS CTH product and the lapse rate method have also been labelled with distinct markers. Additionally, the inset map of Fig. 10 shows the MODIS CTH image on 16 September 2010 at 1710 time, and the green line indicates the CloudSat scanning track. In the cross-section shown in Fig. 10, the MODIS CTH product (black dots) typically underestimates the CTH, and the estimated CTH based on lapse rate method (blue triangles) is more consistent with the CPR-CALIOP observations. Our method performs better in both single-layer and multi-layer clouds.

The retrieved CBH (red triangles) also shows good agreement with the active measurements, even providing perfectly consistent values for deep convective clouds with large geometrical thicknesses. Some previous CBH retrieval algorithms are usually not directly available for deep convective clouds, and lifting condensation levels have been additionally used to determine the CBH of deep convective clouds (Tan et al., 2021; Tan et al., 2023). However, the errors of CBH for multi-layer clouds are still relative larger, with the retrieved values are normally between the upper-layer CBH and the lower-layer CBH. Our method is developed by only single-layer clouds, and the MODIS cloud product exhibits larger errors when multilayer clouds are present. Currently, cloud property retrieval algorithms for passive radiometers typically assume that all cloud pixels are single-layered and homogeneous (Baum et al., 2012; Letu et al., 2019; Platnick et al., 2017). When multilayer clouds are present, the optically thick upper cloud would prevent satellites from detecting the signals of lower clouds, and the lower water clouds also make the detection of upper optically thin ice clouds difficult (Wang et al., 2019; Watts et al., 2011). These may have resulted in the inaccuracy cloud height retrieval results for the multilayer clouds.

4.3. *Applications on geostationary satellites*

In this section, we further extended the method to cloud height retrievals of geostationary satellites (H8 and GOES-13). It's important to note that the lapse rate information is derived from the collocated active-passive satellites data. Factors such as spectral measurement, observation geometry, instrument resolution and retrieval algorithms all contribute to the differences in the accuracy of different satellite products, which will be reflected in the lapse rate. Therefore, the lapse rate was reconstructed separately when applying the method to other passive satellites. However, the fundamental idea of our method remains completely consistent. The collocated H8 and CloudSat samples during 2015 to 2017 were randomly divided into training and validation datasets for method construction and validation, respectively. The AHI

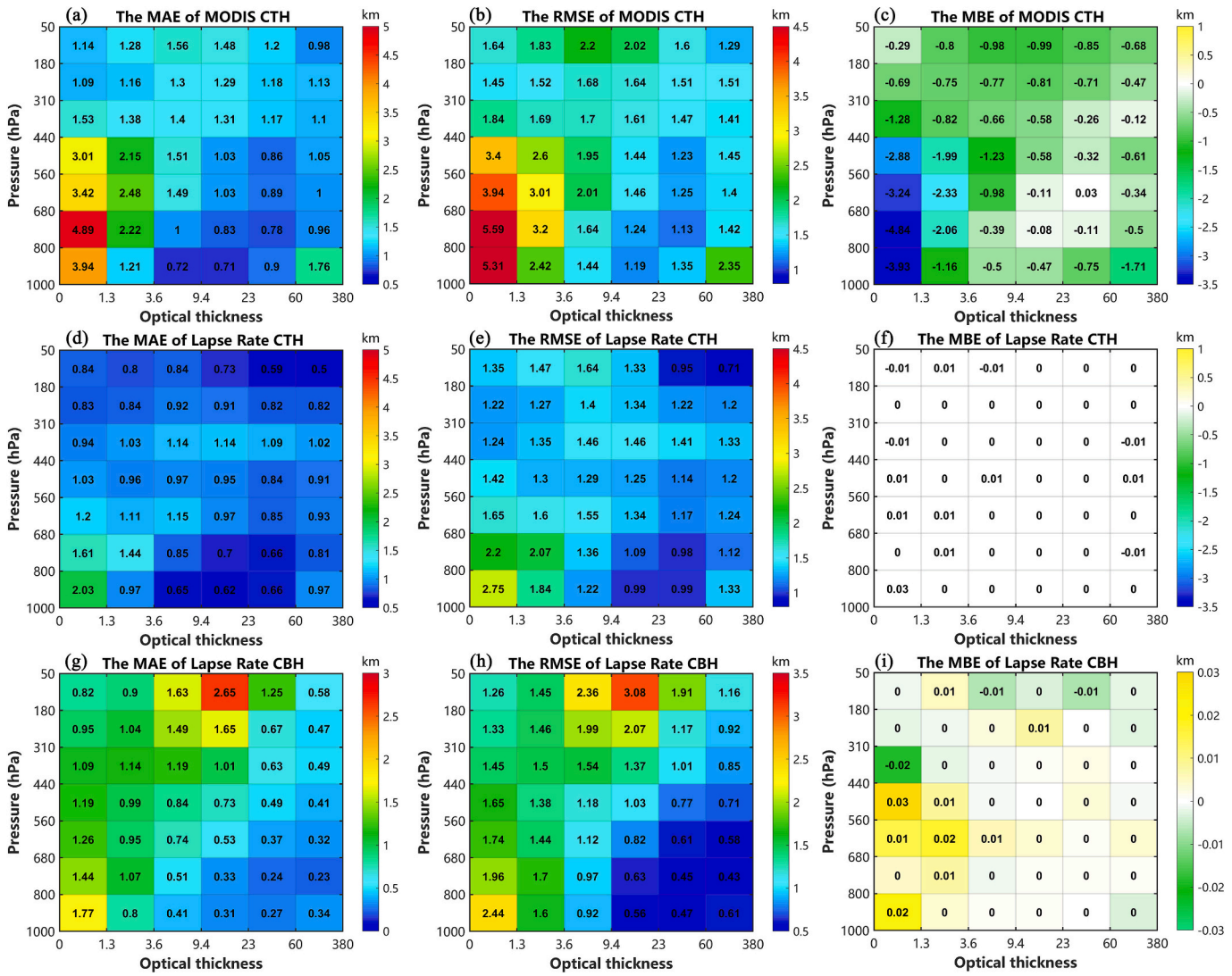

Fig. 9. The joint histogram of CTP and COT for (a, d, g) MAE, (b, e, h) RMSE, and (c, f, i) MBE. The first row is the results of MODIS CTH, the second row is the results of CTH retrieval, and the third row is the results of CBH retrieval. The number in each box expresses the value of the corresponding metric.

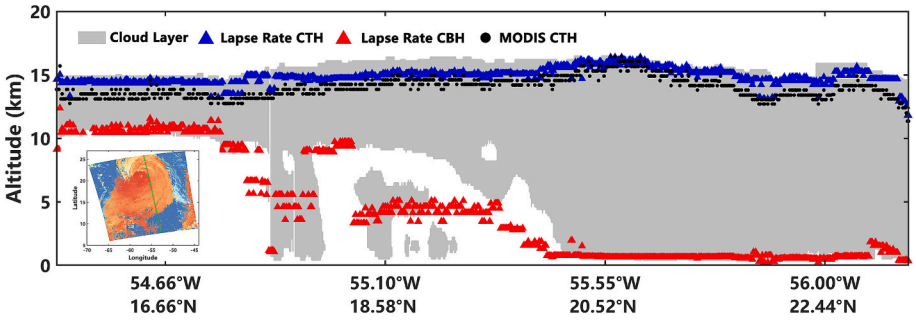

Fig. 10. The inter-comparisons of MODIS CTH product, and our CTH and CBH results with CC for a hurricane scene on September 16, 2010 (17:10 UTC). The gray shading indicates cloud layers derived from CC. The MODIS CTH (black dots), retrieved CTH (blue triangles) and CBH (red triangles) are also displayed. (For interpretation of the references to colour in this figure legend, the reader is referred to the web version of this article.)

pixels closest (within 8 km) to the CloudSat footprint within a time difference of ±5 min were taken as a matching point with observations. For the SatCORPs GEO datasets used in this study, the nighttime COT can be derived by infrared split-window technique (Minnis et al., 2011), so the results in this section are for the whole day.

Fig. 11 shows the validation results of our method on H8 satellite. It can be found that the SatCORPs H8 CTH product has significant biases (MAE = 1.76 km and RMSE = 3.12 km) compared with the active observations (Fig.11a). The SatCORPs products use the CERES Ed4 retrieval algorithms, which determines CTH using a set of parameterizations based on cloud emissivity, cloud effective temperatures and COT (Minnis et al., 2011). The cloud thickness is computed using empirical

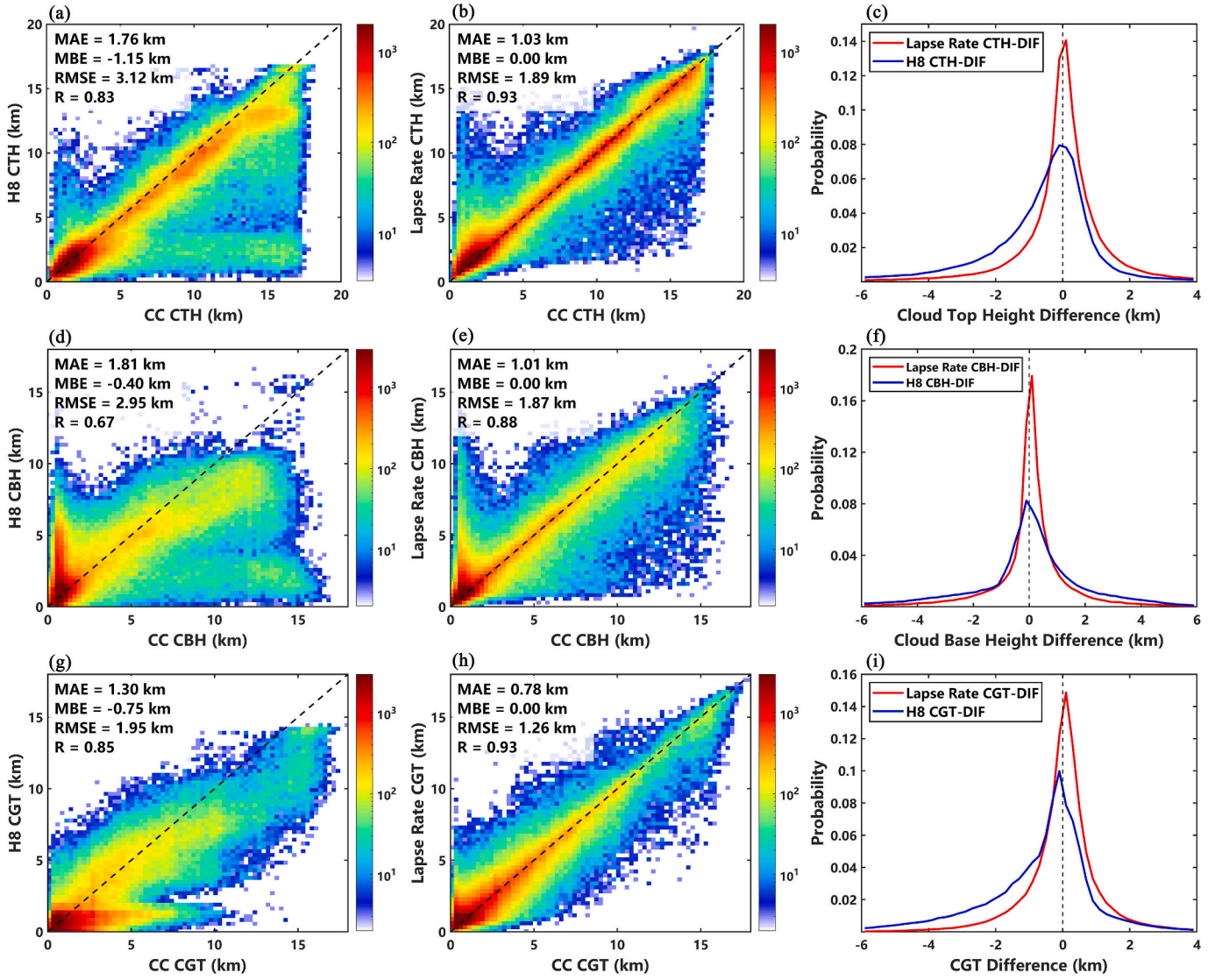

Fig. 11. The validation of CTH, CBH and CGT from SatCORPs H8 product and our retrieval results using active satellite observations for (a) H8 CTH, (b) retrieved CTH, (d) H8 CBH, (e) retrieved CBH, (g) H8 CGT and (h) retrieved CGT. (c) The probability distribution of CTH differences between observations and H8 CTH (blue line), and retrieved CTH (red line). (f) and (i) are same as (c) but for CBH and CGT, respectively. (For interpretation of the references to colour in this figure legend, the reader is referred to the web version of this article.)

formulas based on COT and cloud effective temperatures, and then the CBH is estimated by subtracting cloud thickness from CTH (Minnis et al., 2021). In general, there is an underestimation in CTH, particularly for high clouds, with the MBE of −1.15 km. The SatCORPs H8 CBH product also exhibits an obvious bias, with an overestimation of the low CBH and an underestimation of the high CBH (Fig. 11d). The values of MAE, RMSE and R are 1.81 km, 2.95 km and 0.67, respectively. In comparison, the lapse rate method performs well in both CTH and CBH estimations, with most of the samples clearly concentrated around the 1:1 line. For CTH retrieval, our method effectively alleviates the underestimation for high clouds. All four statistical indicators show significant improvement, with the values of MAE, MBE, RMSE and R are 1.03 km, 0 km,1.89 km and 0.93 respectively (Fig. 11b). Our results are slight superior to the accuracy reported by Min et al. (2020), who developed a gradient boosting decision tree (GBDT) model to derive CTH for the AHI, and the MAE, MBE and RMSE of their results for single-layer clouds are 1.47 km, 0.65 km and 2.39 km, respectively. Based on the Extreme Gradient Boosting (XGBoost) model, Yang et al. (2022) also constructed a CTH retrieval algorithm for AHI using substantial number of spectral information and atmospheric parameters, and our results are also comparable to their accuracy of single-layer clouds (MAE = 1.02 km, MBE = −0.22 km and RMSE = 1.7 km). A marked improvement in the accuracy of retrieved CBH can also be found in various height ranges, our retrieval results have smaller errors (MAE = 0.99 km, MBE = 0 km and RMSE = 1.87 km) and higher consistency ($R = 0.88$) (Fig. 11e). The probability of the CBH deviation can also demonstrate the excellent performance of the lapse rate method, with approximately 71 % of the samples having an absolute error of less than 1 km, significantly better than the 53 % for the H8 product (Fig. 11f). In comparison, our method has comparable performance with that of Tan et al. (2021), who presented a CBH estimation method for Himawari-8 using random forest algorithm, and their retrieval results for single-layer non-precipitation clouds had the best performance with the MBE of −0.2 km.

The validation of CGT estimation derived from CTH and CBH is also shown in Fig. 11g-i. Compared with the statistic results of the CGT derived from SatCORPs H8 product (MAE = 1.30 km, MBE = −0.75 km, RMSE = 1.95 km and $R = 0.85$), our CGT results have smaller errors, the values of MAE, MBE, RMSE and R are 0.78 km, 0 km, 1.26 km and 0.93 (Fig. 11h). The CGT derived from lapse rate method mitigates the underestimation in CGT, and more samples having an absolute error of less

than 1 km (Fig. 11i). Tan et al. (2023) also obtained the CGT estimations for AHI by using the effective cloud water content lookup table, and the MBE and R of their single-layer clouds results are −0.45 km and 0.81, respectively. It can be found that the lapse rate method also has a superior performance in estimating CGT. Here, it is noteworthy that the accuracy of CGT is even higher than that of CTH and CBH. This may be attributed to the error cancellation in CTH and CBH, resulting in a more accurate estimation for CGT.

Similarly, we have also extended the lapse rate method to the GOES-13 satellite, the results are shown in Fig. S6. Similarly, the GOES-13 data closest (within 8 km) to the CC within a time difference of ±10 min was taken as a matching point with observations. The cloud height product of GOES-13 used in this paper has a similar performance to the H8 product, as they are both derived from SatCORPs algorithm. In general, GOES-13 has larger errors than H8 due to fewer observation channels. Similarly, the lapse rate method also performs well on GOES-13 satellite, with both CTH and CBH demonstrating high consistency with active observations. There are also significant improvements in the statistical metrics of cloud height estimations. The MAE, MBE, RMSE and R of retrieved CTH (CBH) are 1.20 km (1.17 km), 0 km (0.01 km), 2.11 km (2.03 km) and 0.91 (0.84), respectively. The CGT estimation derived from retrieved CTH and CBH also agrees well with active observations ($R = 0.92$), and has smaller errors (MBE = 0 km and RMSE = 1.32 km). In conclusion, the lapse rate method maintains high accuracy and stability when applied to different passive satellites.

5. Conclusions and summary

Accurate cloud height information is the basic requirement for understanding the role of clouds on the Earth's climate system and is a prerequisite for improving radiation and precipitation simulations. At present, the operational CTH products from passive satellite measurements are typically significantly biased, and due to obscuration of clouds, accurate CBH products are also highly scarce. In this study, we have developed an effective method to retrieve CTH and CBH for passive sensors based on lapse rate information. Firstly, we constructed a collocated active-passive observation dataset by data matching, and the optimal lapse rate information for different environmental conditions and cloud types were obtained by combining cloud heights from active satellites and temperature information from passive satellites. After that, the mean lapse rate information from the surface to the cloud top (Γ_{ct}) was utilized to determine the CTH, while the lapse rates within (Γ_{cb1}) and below cloud (Γ_{cb2}) were employed to estimate the CBH. Finally, the retrieval accuracy of the lapse rate method was independently evaluated using active observations.

The retrieval results show that the lapse rate method can achieve high accuracy in estimating both CTH and CBH for MODIS. Compared with MODIS CTH product, our algorithm clearly alleviates the CTH underestimation, and all statistical metrics have been improved. With MAE and RMSE decreasing from 1.12 km and 1.72 km to 0.85 km and 1.33 km, respectively. And the MBE and R improved from −0.62 km and 0.94 to 0 km and 0.96, respectively. The retrieved CBH is also in good agreement with those from active measurements ($R = 0.91$), with small deviations (MAE = 0.73 km, MBE = 0 km and RMSE = 1.26 km). In addition, the CGT derived from the retrieved CTH and CBH also agrees well with observations, with MAE and RMSE of 0.97 km and 1.44 km, respectively. Our method is robust and performs well across different seasons, regions, and cloud types, and the retrieved CTH is consistently more accurate than MODIS product. Compared with some previous studies that are only available during the daytime, our method also shows good performance in the retrieval of CTH and CBH at nighttime.

The lapse rate method can also be easily applied to other passive sensors. We have extended the method to cloud height retrieval for both the H8 and GOES-13 satellites, and the results are highly accurate and stable. The MAE and RMSE of H8 CTH (CBH) retrieval results are reduced by 41.5 % (44.2 %) and 39.4 % (36.6 %), respectively, compared with the SatCORPS H8 product. Meanwhile, the correlation coefficient of CTH (CBH) has also increased from 0.83(0.67) to 0.93 (0.88), and the H8 CGT derived from the retrieved CTH and CBH also demonstrated a robust accuracy (MBE = 0 km and $R = 0.93$). In addition, the lapse rate method also performs well on GOES-13 satellite. In summary, our lapse rate method demonstrates high retrieval accuracy and stability in estimating cloud heights during both daytime and nighttime, and has obvious potential for application to other satellites. Lapse rate method is also very convenient, as CTH and CBH can be retrieved based on only several variables from passive satellites. In the meantime, the performance of our method is also comparable to that of machine learning methods that use a substantial number of spectral signals and atmospheric parameters.

Nevertheless, as we mentioned earlier, the lapse rate method proposed in this study also has some limitations and uncertainties. Firstly, the retrieval bias of properties (e.g. CTT and ST) from passive sensors can affect the accuracy of our method. In the MODIS product, CTT and CTH are correspond to each other, so the CTH bias can be used to represent the CTT bias. When samples are constrained with CTH bias less than 2.5 km, the retrieval accuracy improves significantly, with the RMSE of CTH (CBH) retrievals reducing from 1.33 km (1.26 km) to 0.82 km (1.03 km) at daytime. Specifically, the presence of multilayer clouds would significantly affect the retrieval of cloud top properties from passive sensors (Chang and Li, 2005; Min et al., 2017), which further affects the performance of our method. In particularly, previous studies have shown that subvisible cirrus clouds with small optical thickness and strong radiative effect are widely found in the atmosphere (Sun et al., 2015; Sun et al., 2011). These clouds are usually undetectable by passive sensors, significantly affecting the retrieval of cloud top and surface temperature from passive observations (Sun et al., 2011), and hence the accuracy of our method. Although some previous studies have developed multilayer cloud detection algorithms based on multichannel information or machine learning methods (Tan et al., 2022; Wang et al., 2019), and have derived the cloud properties of specific overlapping cloud types using the combined microwave and visible-infrared measurements (Huang et al., 2006) or multispectral measurements (Huang et al., 2005; Teng et al., 2023), these methods still have some limitations. Therefore, the detection and properties retrieval of multilayer clouds have so far remained highly desirable but extremely challenging. Future studies should focus on the development of more accurate algorithm for detection and properties retrieval of multilayer clouds by combining active satellites observations, multispectral measurements and meteorological conditions. Moreover, precipitation can also affect the CBH estimations. However, passive satellites continue to present difficulties in accurately identifying precipitation (Kühnlein et al., 2014; Min et al., 2019). Recently, some studies have developed highly accurate precipitation identification and quantitative precipitation estimation algorithms by combining cloud properties, meteorological factors, and visible/infrared spectral signals (Li et al., 2021; Zhu and Ma, 2022). These algorithms will contribute to the future enhancement of lapse rate method by distinguishing precipitation clouds from non-precipitation clouds and retrieve their cloud height separately.

At present, radiosondes can provide reliable measurements of the relative humidity (RH) and air temperature (T) at numerous global stations, allowing for the vertical distribution of clouds to be determined. The method of using relative humidity thresholds to detect cloud vertical structure from radiosonde observations has been widely applied (Wang and Rossow, 1995; Zhang et al., 2010). However, relying solely on the humidity threshold indicator may lead to misjudgments of cloud layers, and fixed humidity thresholds are also not suitable for different regions globally (Costa-Surós et al., 2014). In fact, there are significant differences in temperature changes inside and outside of cloud layers. Chernykh and Eskridge (1996) presented a method to determine cloud boundaries using the second derivatives of RH and T. In this investigation, our results have also revealed significant variations of the lapse

rates inside and outside of clouds, along with distinct spatiotemporal distribution patterns. It means that the lapse rate method can serve as a supplemental criterion to the existing relative humidity threshold method to identify more accurate cloud boundaries for radiosonde observations.

CRediT authorship contribution statement

Weiyuan Zhang: Writing – original draft, Visualization, Methodology, Investigation, Data curation. **Jiming Li:** Writing – review & editing, Validation, Supervision, Project administration, Methodology, Conceptualization. **Jiayi Li:** Visualization, Software, Data curation. **Sihang Xu:** Investigation, Data curation. **Lijie Zhang:** Software, Data curation. **Yang Wang:** Writing – review & editing. **Jianping Huang:** Writing – review & editing, Supervision, Project administration.

Declaration of Competing Interest

The authors declare that they have no known competing financial interests or personal relationships that could have appeared to influence the work reported in this paper.

Acknowledgments

This research was jointly supported by the key Program of the National Natural Science Foundation of China (42430601) and the Major Program of the National Natural Science Foundation of China (42090030). The authors declare that they have no conflicts of interest. We would like to appreciate the CloudSat, MODIS, SatCORPs GEO, and ERA5 science teams for providing excellent and accessible data products that made this study possible.

Appendix A. Supplementary data

Supplementary data to this article can be found online at https://doi.org/10.1016/j.rse.2025.114622.

Data availability

Data will be made available on request.

References

Adhikari, A., Talukdar, S., Maitra, A., 2017. Rain drop size variation with cloud base height at a tropical location. Indian J. Phys. 91 (5), 481–488. https://doi.org/10.1007/s12648-016-0936-4.

Barker, H.W., Jerg, M.P., Wehr, T., Kato, S., Donovan, D.P., Hogan, R.J., 2011. A 3D cloud-construction algorithm for the EarthCARE satellite mission. Quart. J. Roy. Meteor. Soc. 137 (657), 1042–1058. https://doi.org/10.1002/qj.824.

Baum, B.A., Menzel, W.P., Frey, R.A., Tobin, D.C., Holz, R.E., Ackerman, S.A., Heidinger, A.K., Yang, P., 2012. MODIS cloud-top property refinements for collection 6. J. Appl. Meteorol. Climatol. 51 (6), 1145–1163. https://doi.org/10.1175/jamc-d-11-0203.1.

Bertrand, L., Kay, J.E., Haynes, J., de Boer, G., 2024. A global gridded dataset for cloud vertical structure from combined cloudsat and calipso observations. Earth Syst. Sci. Data 16 (3), 1301–1316. https://doi.org/10.5194/essd-16-1301-2024.

Bessho, K., Date, K., Hayashi, M., Ikeda, A., Imai, T., Inoue, H., Kumagai, Y., Miyakawa, T., Murata, H., Ohno, T., Okuyama, A., Oyama, R., Sasaki, Y., Shimazu, Y., Shimoji, K., Sumida, Y., Suzuki, M., Taniguchi, H., Tsuchiyama, H., Uesawa, D., Yokota, H., Yoshida, R., 2016. An introduction to Himawari-8/9-japan's new-generation geostationary meteorological satellites. J. Meteorol. Soc. Japan.Ser. II. 94 (2), 151–183. https://doi.org/10.2151/jmsj.2016-009.

Biondi, R., Ho, S.P., Randel, W., Syndergaard, S., Neubert, T., 2013. Tropical cyclone cloud-top height and vertical temperature structure detection using GPS radio occultation measurements. J. Geophys. Res.-Atmos. 118 (11), 5247–5259. https://doi.org/10.1002/jgrd.50448.

Cesana, G., Waliser, D.E., Henderson, D., L'Ecuyer, T.S., Jiang, X., Li, J.L.F., 2019. The vertical structure of radiative heating rates: a multimodel evaluation using A-train satellite observations. J. Clim. 32 (5), 1573–1590. https://doi.org/10.1175/jcli-d-17-0136.1.

Chang, F.L., Li, Z.Q., 2005. A new method for detection of cirrus overlapping water clouds and determination of their optical properties. J. Atmos. Sci. 62 (11), 3993–4009. https://doi.org/10.1175/jas3578.1.

Chen, T., Rossow, W.B., Zhang, Y.C., 2000. Radiative effects of cloud-type variations. J. Clim. 13 (1), 264–286. https://doi.org/10.1016/j.rse.2024.114319.

Chernykh, I.V., Eskridge, R.E., 1996. Determination of cloud amount and level from radiosonde soundings. J. Appl. Meteorol. Climatol. 35 (8), 1362–1369.

Chi, Y.L., Zhao, C.F., Yang, Y.K., Zhao, X., Yang, J., 2024. Global characteristics of cloud macro-physical properties from active satellite remote sensing. Atmos. Res. 302, 19. https://doi.org/10.1016/j.atmosres.2024.107316.

Cho, H.M., Zhang, Z.B., Meyer, K., Lebsock, M., Platnick, S., Ackerman, A.S., Di Girolamo, L., C-Labonnote, L., Cornet, C., Riedi, J., Holz, R.E., 2015. Frequency and causes of failed modis cloud property retrievals for liquid phase clouds over global oceans. J. Geophys. Res.-Atmos. 120 (9), 4132–4154. https://doi.org/10.1002/2015jd023161.

Costa-Surós, M., Calbó, J., González, J.A., Long, C.N., 2014. Comparing the cloud vertical structure derived from several methods based on radiosonde profiles and ground-based remote sensing measurements. Atmos. Meas. Tech. 7 (8), 2757–2773. https://doi.org/10.5194/amt-7-2757-2014.

Dong, X.Q., Minnis, P., Xi, B., Sun, S., Chen, Y., 2008. Comparison of CERES-MODIS stratus cloud properties with ground-based measurements at the DOE ARM southern great plains site. J. Geophys. Res.-Atmos. 113 (D3), 17. https://doi.org/10.1029/2007jd008438.

Forsythe, J.M., Vonder Haar, T.H., Reinke, D.L., 2000. Cloud-base height estimates using a combination of meteorological satellite imagery and surface reports. J. Appl. Meteorol. 39 (12), 2336–2347.

Håkansson, N., Adok, C., Thoss, A., Scheirer, R., Hörnquist, S., 2018. Neural network cloud top pressure and height for MODIS. Atmos. Meas. Tech. 11 (5), 3177–3196. https://doi.org/10.5194/amt-11-3177-2018.

Hamann, U., Walther, A., Baum, B., Bennartz, R., Bugliaro, L., Derrien, M., Francis, P.N., Heidinger, A., Joro, S., Kniffka, A., Le Gléau, H., Lockhoff, M., Lutz, H.J., Meirink, J. F., Minnis, P., Palikonda, R., Roebeling, R., Thoss, A., Platnick, S., Watts, P., Wind, G., 2014. Remote sensing of cloud top pressure/height from SEVIRI: analysis of ten current retrieval algorithms. Atmos. Meas. Tech. 7 (9), 2839–2867. https://doi.org/10.5194/amt-7-2839-2014.

Hartmann, D.L., Ockertbell, M.E., Michelsen, M.L., 1992. The effect of cloud type on earths energy-balance - global analysis. J. Clim. 5 (11), 1281–1304.

Haynes, J.M., Vonder Haar, T.H., L'Ecuyer, T., Henderson, D., 2013. Radiative heating characteristics of earth's cloudy atmosphere from vertically resolved active sensors. Geophys. Res. Lett. 40 (3), 624–630. https://doi.org/10.1002/grl.50145.

Heidinger, A.K., Pavolonis, M.J., 2009. Gazing at cirrus clouds for 25 years through a split window. Part I: Methodol. J. Appl. Meteorol. Climatol. 48 (6), 1100–1116. https://doi.org/10.1175/2008jamc1882.1.

Hersbach, H., Bell, B., Berrisford, P., Hirahara, S., Horányi, A., Muñoz-Sabater, J., Nicolas, J., Peubey, C., Radu, R., Schepers, D., Simmons, A., Soci, C., Abdalla, S., Abellan, X., Balsamo, G., Bechtold, P., Biavati, G., Bidlot, J., Bonavita, M., De Chiara, G., Dahlgren, P., Dee, D., Diamantakis, M., Dragani, R., Flemming, J., Forbes, R., Fuentes, M., Geer, A., Haimberger, L., Healy, S., Hogan, R.J., Hólm, E., Janisková, M., Keeley, S., Laloyaux, P., Lopez, P., Lupu, C., Radnoti, G., de Rosnay, P., Rozum, I., Vamborg, F., Villaume, S., Thépaut, J.N., 2020. The ERA5 global reanalysis. Quart. J. Roy. Meteor. Soc. 146 (730), 1999–2049. https://doi.org/10.1002/qj.3803.

Holz, R.E., Ackerman, S.A., Nagle, F.W., Frey, R., Dutcher, S., Kuehn, R.E., Vaughan, M. A., Baum, B., 2008. Global moderate resolution imaging Spectroradiometer (MODIS) cloud detection and height evaluation using CALIOP. J. Geophys. Res.-Atmos. 113, 17. https://doi.org/10.1029/2008jd009837.

Huang, J.P., Minnis, P., Lin, B., Yi, Y.H., Khaiyer, M.M., Arduini, R.F., Fan, A., Mace, G. G., 2005. Advanced retrievals of multilayered cloud properties using multispectral measurements. J. Geophys. Res.-Atmos. 110 (D15), 12. https://doi.org/10.1029/2004jd005101.

Huang, J.P., Minnis, P., Lin, B., Yi, Y.H., Fan, T.F., Sun-Mack, S., Ayers, J.K., 2006. Determination of ice water path in ice-over-water cloud systems using combined MODIS and AMSR-E measurements. Geophys. Res. Lett. 33 (21), 5. https://doi.org/10.1029/2006gl027038.

Huo, J., Li, J., Duan, M.Z., Lv, D.R., Han, C.Z., Bi, Y.H., 2020a. Measurement of cloud top height: comparison of MODIS and ground-based millimeter radar. Remote Sens. 12 (10), 17. https://doi.org/10.3390/rs12101616.

Huo, J., Lu, D.R., Duan, S., Bi, Y.H., Liu, B., 2020b. Comparison of the cloud top heights retrieved from MODIS and AHI satellite data with ground-based Ka-band radar. Atmos. Meas. Tech. 13 (1), 1–11. https://doi.org/10.5194/amt-13-1-2020.

Hutchison, K.D., 2002. The retrieval of cloud base heights from MODIS and three-dimensional cloud fields from NASA's EOS aqua mission. Int. J. Remote Sens. 23 (24), 5249–5265. https://doi.org/10.1080/01431160110117391.

Hutchison, K.D., Wong, E., Ou, S.C., 2006. Cloud base heights retrieved during night-time conditions with MODIS data. Int. J. Remote Sens. 27, 2847–2862.

Iwabuchi, H., Putri, N.S., Saito, M., Tokoro, Y., Sekiguchi, M., Yang, P., Baum, B.A., 2018. Cloud property retrieval from multiband infrared measurements by Himawari-8. J. Meteorol. Soc. Japan.Ser.II 96B, 27–42. https://doi.org/10.2151/jmsj.2018-001.

Jakob, C., Schumacher, C., 2008. Precipitation and latent heating characteristics of the major tropical western pacific cloud regimes. J. Clim. 21 (17), 4348–4364. https://doi.org/10.1175/2008jcli2122.1.

King, J.M., Kummerow, C.D., van den Heever, S.C., Igel, M.R., 2015. Observed and modeled warm rainfall occurrence and its relationships with cloud macrophysical properties. J. Atmos. Sci. 72 (11), 4075–4090. https://doi.org/10.1175/jas-d-14-0368.1.

King, M.D., Menzel, W.P., Kaufman, Y.J., Tanré, D., Gao, B.C., Platnick, S., Ackerman, S. A., Remer, L.A., Pincus, R., Hubanks, P.A., 2003. Cloud and aerosol properties, precipitable water, and profiles of temperature and water vapor from MODIS. IEEE

Trans. Geosci. Remote Sens. 41 (2), 442–458. https://doi.org/10.1109/tgrs.2002.808226.
Kühnlein, M., Appelhans, T., Thies, B., Nauss, T., 2014. Improving the accuracy of rainfall rates from optical satellite sensors with machine learning - a random forests-based approach applied to MSG SEVIRI. Remote Sens. Environ. 141, 129–143. https://doi.org/10.1016/j.rse.2013.10.026.
Letu, H.S., Nagao, T.M., Nakajima, T.Y., Riedi, J., Ishimoto, H., Baran, A.J., Shang, H.Z., Sekiguchi, M., Kikuchi, M., 2019. Ice cloud properties from Himawari-8/ahi next-generation geostationary satellite: capability of the AHI to monitor the DC cloud generation process. IEEE Trans. Geosci. Remote Sens. 57 (6), 3229–3239. https://doi.org/10.1109/tgrs.2018.2882803.
Li, J.D., You, Q.L., He, B., 2020. Distinctive spring shortwave cloud radiative effect and its inter-annual variation over southeastern China. Atmos. Sci. Lett. 21 (6), 8. https://doi.org/10.1002/asl.970.
Li, J.M., Yi, Y.H., Minnis, P., Huang, J.P., Yan, H.R., Ma, Y.J., Wang, W.C., Ayers, J.K., 2011. Radiative effect differences between multi-layered and single-layer clouds derived from CERES, CALIPSO, and CloudSat data. J. Quant. Spectrosc. Radiat. Transf. 112 (2), 361–375. https://doi.org/10.1016/j.jqsrt.2010.10.006.
Li, J.M., Yi, Y.H., Stamnes, K., Ding, X.D., Wang, T.H., Jin, H.C., Wang, S.S., 2013. A new approach to retrieve cloud base height of marine boundary layer clouds. Geophys. Res. Lett. 40 (16), 4448–4453. https://doi.org/10.1002/grl.50836.
Li, S., Yang, J., 2024. Retrieving global single-layer liquid cloud thickness from OCO-2 hyperspectral oxygen A-band. Remote Sens. Environ. 311, 114272.
Li, X.Y., Yang, Y.J., Mi, J.Q., Bi, X.Y., Zhao, Y., Huang, Z.H., Liu, C., Zong, L., Li, W.J., 2021. Leveraging machine learning for quantitative precipitation estimation from Fengyun-4 geostationary observations and ground meteorological measurements. Atmos. Meas. Tech. 14 (11), 7007–7023. https://doi.org/10.5194/amt-14-7007-2021.
Liang, Y., Sun, X.J., Miller, S.D., Li, H.R., Zhou, Y.B., Zhang, R.W., Li, S.H., 2017. Cloud base height estimation from ISCCP cloud-type classification applied to a-train data. Adv. Meteorol. 2017, 14. https://doi.org/10.1155/2017/3231719.
Lin, H., Li, Z.L., Li, J., Zhang, F., Min, M., Menzel, W.P., 2022. Estimate of daytime single-layer cloud base height from advanced baseline imager measurements. Remote Sens. Environ. 274, 15. https://doi.org/10.1016/j.rse.2022.112970.
Liou, K.N., 2002. An Introduction to Atmospheric Radiation, 2 ed. New York, USA, Academic Press.
Lu, X., Mao, F.Y., Rosenfeld, D., Zhu, Y.N., Pan, Z.X., Gong, W., 2021. Satellite retrieval of cloud base height and geometric thickness of low-level cloud based on CALIPSO. Atmos. Chem. Phys. 21 (15), 11979–12003. https://doi.org/10.5194/acp-21-11979-2021.
Luo, H., Quaas, J., Han, Y., 2023. Examining cloud vertical structure and radiative effects from satellite retrievals and evaluation of CMIP6 scenarios. Atmos. Chem. Phys. 23 (14), 8169–8186. https://doi.org/10.5194/acp-23-8169-2023.
Mace, G.G., Zhang, Q.Q., 2014. The CloudSat radar-lidar geometrical profile product (RL-GeoProf): updates, improvements, and selected results. J. Geophys. Res.-Atmos. 119 (15), 9441–9462. https://doi.org/10.1002/2013jd021374.
Mace, G.G., Zhang, Q.Q., Vaughan, M., Marchand, R., Stephens, G., Trepte, C., Winker, D., 2009. A description of hydrometeor layer occurrence statistics derived from the first year of merged CloudSat and CALIPSO data. J. Geophys. Res.-Atmos. 114, 17. https://doi.org/10.1029/2007jd009755.
Mather, J.H., McFarlane, S.A., Miller, M.A., Johnson, K.L., 2007. Cloud properties and associated radiative heating rates in the tropical western pacific. J. Geophys. Res.-Atmos. 112 (D5), 19. https://doi.org/10.1029/2006jd007555.
McFarlane, S.A., Mather, J.H., Ackerman, T.P., 2007. Analysis of tropical radiative heating profiles: a comparison of models and observations. J. Geophys. Res.-Atmos. 112 (D14). https://doi.org/10.1029/2006jd008290.
McKee, T., Cox, S.K., 1976. Simulated radiance patterns for finite cubic clouds. J. Atmos. 33 (10), 2014–2020.
Mecikalski, J.R., Feltz, W.F., Murray, J.J., Johnson, D.B., Bedka, K.M., Bedka, S.T., Wimmers, A.J., Pavolonis, M., Berendes, T.A., Haggerty, J., Minnis, P., Bernstein, B., Williams, E., 2007. Aviation applications for satellite-based observations of cloud properties, convection initiation, in-flight icing, turbulence, and volcanic ash. B. Am. Meteorol. Soc. 88, 1589–1607. URL: https://journals.ametsoc. org/view/journals/bams/88/10/bams-88-10-1589.xml. https://doi.org/10.1175/BAMS-88-10-1589.
Menzel, W.P., Frey, R.A., Zhang, H., Wylie, D.P., Moeller, C.C., Holz, R.E., Maddux, B., Baum, B.A., Strabala, K.I., Gumley, L.E., 2008. MODIS global cloud-top pressure and amount estimation: algorithm description and results. J. Appl. Meteorol. Climatol. 47 (4), 1175–1198.
Miller, S.D., Forsythe, J.M., Partain, P.T., Haynes, J.M., Bankert, R.L., Sengupta, M., Mitrescu, C., Hawkins, J.D., Vonder Haar, T.H., 2014. Estimating three-dimensional cloud structure via statistically blended satellite observations. J. Appl. Meteorol. Climatol. 53 (2), 437–455. https://doi.org/10.1175/jamc-d-13-070.1.
Min, M., Wu, C.Q., Li, C., Liu, H., Xu, N., Wu, X., Chen, L., Wang, F., Sun, F.L., Qin, D.Y., Wang, X., Li, B., Zheng, Z.J., Cao, G.Z., Dong, L.X., 2017. Developing the science product algorithm testbed for Chinese next-generation geostationary meteorological satellites: Fengyun-4 series. J. Meteorol. Res. 31 (4), 708–719. https://doi.org/10.1007/s13351-017-6161-z.
Min, M., Bai, C., Guo, J.P., Sun, F.L., Liu, C., Wang, F., Xu, H., Tang, S.H., Li, B., Di, D., Dong, L.X., Li, J., 2019. Estimating summertime precipitation from Himawari-8 and global forecast system based on machine learning. IEEE Trans. Geosci. Remote Sens. 57 (5), 2557–2570. https://doi.org/10.1109/tgrs.2018.2874950.
Min, M., Li, J., Wang, F., Liu, Z.J., Menzel, W.P., 2020. Retrieval of cloud top properties from advanced geostationary satellite imager measurements based on machine learning algorithms. Remote Sens. Environ. 239, 20. https://doi.org/10.1016/j.rse.2019.111616.
Minnis, P., Nguyen, L., Palikonda, R., Heck, P.W., Spangenberg, D.A., Doelling, D.R., Ayers, J.K., Smith Jr., W.L., Khaiyer, M.M., Trepte, Q.Z., Avey, L.A., Chang, F.-L., Yost, C.R., Chee, T.L., Sun-Mack, S., 2008. Near-real time cloud retrievals from operational and research meteorological satellites. In: Presented at the SPIE Remote Sensing, Cardiff, Wales, United Kingdom, p. 710703. https://doi.org/10.1117/12.800344.
Minnis, P., Sun-Mack, S., Young, D.F., Heck, P.W., Garber, D.P., Chen, Y., Spangenberg, D.A., Arduini, R.F., Trepte, Q.Z., Smith, W.L., Ayers, J.K., Gibson, S.C., Miller, W.F., Hong, G., Chakrapani, V., Takano, Y., Liou, K.N., Xie, Y., Yang, P., 2011. CERES Edition-2 cloud property retrievals using TRMM VIRS and Terra and Aqua MODIS data-part I: algorithms. IEEE Trans. Geosci. Remote Sens. 49 (11), 4374–4400. https://doi.org/10.1109/tgrs.2011.2144601.
Minnis, P., Sun-Mack, S., Chen, Y., Chang, F.L., Yost, C.R., Smith, W.L., Heck, P.W., Arduini, R.F., Bedka, S.T., Yi, Y.H., Hong, G., Jin, Z.H., Painemal, D., Palikonda, R., Scarino, B.R., Spangenberg, D.A., Smith, R.A., Trepte, Q.Z., Yang, P., Xie, Y., 2021. CERES MODIS cloud product retrievals for edition 4-part I: algorithm changes. IEEE Trans. Geosci. Remote Sens. 59 (4), 2744–2780. https://doi.org/10.1109/tgrs.2020.3008866.
Mülmenstädt, J., Sourdeval, O., Henderson, D.S., L'Ecuyer, T.S., Unglaub, C., Jungandreas, L., Böhm, C., Russell, L.M., Quaas, J., 2018. Using CALIOP to estimate cloud-field base height and its uncertainty: the Cloud Base altitude spatial extrapolator (CBASE) algorithm and dataset. Earth Syst. Sci. Data 10 (4), 2279–2293. https://doi.org/10.5194/essd-10-2279-2018.
Naud, C.M., Baum, B.A., Pavolonis, M., Heidinger, A., Frey, R., Zhang, H., 2007. Comparison of MISR and MODIS cloud-top heights in the presence of cloud overlap. Remote Sens. Environ. 107 (1–2), 200–210. https://doi.org/10.1016/j.rse.2006.09.030.
Noh, Y.J., Forsythe, J.M., Miller, S.D., Seaman, C.J., Li, Y., Heidinger, A.K., Lindsey, D.T., Rogers, M.A., Partain, P.T., 2017. Cloud-base height estimation from VIIRS. Part II: a statistical algorithm based on A-train satellite data. J. Atmos. Ocean. Technol. 34 (3), 585–598. https://doi.org/10.1175/jtech-d-16-0110.1.
Platnick, S., King, M.D., Ackerman, S.A., Menzel, W.P., Baum, B.A., Riédi, J.C., Frey, R. A., 2003. The MODIS cloud products: algorithms and examples from Terra. IEEE Trans. Geosci. Remote Sens. 41 (2), 459–473. https://doi.org/10.1109/tgrs.2002.808301.
Platnick, S., Meyer, K.G., King, M.D., Wind, G., Amarasinghe, N., Marchant, B., Arnold, G.T., Zhang, Z.B., Hubanks, P.A., Holz, R.E., Yang, P., Ridgway, W.L., Riedi, J., 2017. The MODIS cloud optical and microphysical products: collection 6 updates and examples from Terra and Aqua. IEEE Trans. Geosci. Remote Sens. 55 (1), 502–525. https://doi.org/10.1109/tgrs.2016.2610522.
Rajeevan, M., Nanjundiah, R.S., 2009. Coupled model simulations of twentieth century climate of the Indian summer monsoon. In: Platinum Jubilee Special Volume of the Indian Academy of Sciences, 20, pp. 537–568.
Rozanov, V.V., Kokhanovsky, A.A., 2004. Semianalytical cloud retrieval algorithm as applied to the cloud top altitude and the cloud geometrical thickness determination from top-of-atmosphere reflectance measurements in the oxygen A band. J. Geophys. Res.-Atmos. 109 (D5), 21. https://doi.org/10.1029/2003jd004104.
Sassen, K., Campbell, J.R., 2001. A midlatitude cirrus cloud climatology from the facility for atmospheric remote sensing. Part I: macrophysical and synoptic properties. J. Atmos. Sci. 58, 481–496.
Shao, J.Q., Letu, H., Ri, X., Tana, G., Wang, T.X., Shang, H.Z., 2023. Estimation of surface downward longwave radiation and cloud base height based on infrared multichannel data of Himawari-8. Atmosphere 14 (3), 18. https://doi.org/10.3390/atmos14030493.
Simpson, J.J., McIntire, T., Jin, Z.H., Stitt, J.R., 2000. Improved cloud top height retrieval under arbitrary viewing and illumination conditions using AVHRR data. Remote Sens. Environ. 72 (1), 95–110. https://doi.org/10.1016/s0034-4257(99)00095-4.
Stephens, G.L., Vane, D.G., Boain, R.J., Mace, G.G., Sassen, K., Wang, Z.E., Illingworth, A. J., O'Connor, E.J., Rossow, W.B., Durden, S.L., Miller, S.D., Austin, R.T., Benedetti, A., Mitrescu, C., CloudSat Sci, T., 2002. The CloudSat mission and the A-train: a new dimension of space-based observations of clouds and precipitation. Bull. Am. Meteorol. Soc. 83 (12), 1771–1790. https://doi.org/10.1175/bams-83-12-1771.
Stephens, G.L., Vane, D.G., Tanelli, S., Im, E., Durden, S., Rokey, M., Reinke, D., Partain, P., Mace, G.G., Austin, R., L'Ecuyer, T., Haynes, J., Lebsock, M., Suzuki, K., Waliser, D., Wu, D., Kay, J., Gettelman, A., Wang, Z., Marchand, R., 2008. Cloudsat mission: performance and early science after the first year of operation. J. Geophys. Res.-Atmos. 113 (D23). https://doi.org/10.1029/2008jd009982.
Sun, W., Baize, R.R., Videen, G., Hu, Y., Fu, Q., 2015. A method to retrieve super-thin cloud optical depth over ocean background with polarized sunlight. Atmos. Chem. Phys. 15 (20), 11909–11918. https://doi.org/10.5194/acp-15-11909-2015.
Sun, W.B., Videen, G., Kato, S., Lin, B., Lukashin, C., Hu, Y.X., 2011. A study of subvisual clouds and their radiation effect with a synergy of CERES, MODIS, CALIPSO, and AIRS data. J. Geophys. Res.-Atmos. 116, 10. https://doi.org/10.1029/2011jd016422.
Sun, X.J., Li, H.R., Barker, H.W., Zhang, R.W., Zhou, Y.B., Liu, L., 2016. Satellite-based estimation of cloud-base heights using constrained spectral radiance matching. Quart. J. Roy. Meteor. Soc. 142 (694), 224–232. https://doi.org/10.1002/qj.2647.
Sun-Mack, S., Minnis, P., Chen, Y., Kato, S., Yi, Y.H., Gibson, S.C., Heck, P.W., Winker, D. M., 2014. Regional apparent boundary layer lapse rates determined from CALIPSO and MODIS data for cloud-height determination. J. Appl. Meteorol. Climatol. 53 (4), 990–1011. https://doi.org/10.1175/jamc-d-13-081.1.
Tan, Z.H., Ma, S., Zhao, X.B., Yan, W., Lu, W., 2019. Evaluation of cloud top height retrievals from china's next-generation geostationary meteorological satellite FY-4a. J. Meteorol. Res. 33 (3), 553–562. https://doi.org/10.1007/s13351-019-8123-0.

Tan, Z.H., Huo, J., Ma, S., Han, D., Wang, X., Hu, S.S., Yan, W., 2021. Estimating cloud base height from Himawari-8 based on a random forest algorithm. Int. J. Remote Sens. 42 (7), 2485–2501. https://doi.org/10.1080/01431161.2020.1854891.

Tan, Z.H., Liu, C., Ma, S., Wang, X., Shang, J., Wang, J.J., Ai, W.H., Yan, W., 2022. Detecting multilayer clouds from the geostationary advanced himawari imager using machine learning techniques. IEEE Trans. Geosci. Remote Sens. 60, 12. https://doi.org/10.1109/tgrs.2021.3087714.

Tan, Z.H., Ma, S., Liu, C., Teng, S.W., Letu, H., Zhang, P., Ai, W.H., 2023. Retrieving cloud base height from passive radiometer observations via a systematic effective cloud water content table. Remote Sens. Environ. 294, 13. https://doi.org/10.1016/j.rse.2023.113633.

Teng, S.W., Liu, C., Tan, Z.H., Li, J.M., Xu, N., Hu, X.Q., Zhang, P., Yan, W., Sohn, B.J., 2023. A multispectral method for retrieving overlapping cloud top heights from passive radiometers. Remote Sens. Environ. 286, 15. https://doi.org/10.1016/j.rse.2022.113425.

Viúdez-Mora, A., Costa-Surós, M., Calbó, J., González, J.A., 2015. Modeling atmospheric longwave radiation at the surface during overcast skies: the role of cloud base height. J. Geophys. Res.-Atmos. 120 (1), 199–214. https://doi.org/10.1002/2014jd022310.

Wang, J.H., Rossow, W.B., 1995. Determination of cloud vertical structure from upper-air observations. J. Appl. Meteorol. 34 (10), 2243–2258.

Wang, J.J., Liu, C., Yao, B., Min, M., Letu, H.S., Yin, Y., Yung, Y.L., 2019. A multilayer cloud detection algorithm for the Suomi-NPP Visible Infrared Imager Radiometer Suite (VIIRS). Remote Sens. Environ. 227, 1–11. https://doi.org/10.1016/j.rse.2019.02.024.

Wang, Q., Zhou, C., Zhuge, X., Liu, C., Weng, F., Wang, M., 2022. Retrieval of cloud properties from thermal infrared radiometry using convolutional neural network. Remote Sens. Environ. 278. https://doi.org/10.1016/j.rse.2022.113079.

Wang, Q., Zhou, C., Letu, H., Zhu, Y.N., Zhuge, X.Y., Liu, C., Weng, F.Z., Wang, M.H., 2023. Obtaining cloud base height and phase from thermal infrared radiometry using a deep learning algorithm. IEEE Trans. Geosci. Remote Sens. 61, 14. https://doi.org/10.1109/tgrs.2023.3317532.

Watts, P.D., Bennartz, R., Fell, F., 2011. Retrieval of two-layer cloud properties from multispectral observations using optimal estimation. J. Geophys. Res.-Atmos. 116, 22. https://doi.org/10.1029/2011jd015883.

Weisz, E., Li, J., Menzel, W.P., Heidinger, A.K., Kahn, B.H., Liu, C.Y., 2007. Comparison of AIRS, MODIS, CloudSat and CALIPSO cloud top height retrievals. Geophys. Res. Lett. 34 (17), 5. https://doi.org/10.1029/2007gl030676.

Winker, D.M., Vaughan, M.A., Omar, A., Hu, Y.X., Powell, K.A., Liu, Z.Y., Hunt, W.H., Young, S.A., 2009. Overview of the CALIPSO mission and CALIOP data processing algorithms. J. Atmos. Ocean. Technol. 26 (11), 2310–2323. https://doi.org/10.1175/2009jtecha1281.1.

Wu, D., Hu, Y.X., McCormick, M.P., Xu, K.M., Liu, Z.Y., Smith, B., Omar, A.H., Chang, F.L., 2008. Deriving marine-boundary-layer lapse rate from collocated CALIPSO, MODIS, and AMSR-E data to study global low-cloud height statistics. IEEE Geosci. Remote Sens. Lett. 5 (4), 649–652. https://doi.org/10.1109/lgrs.2008.2002024.

Xu, H., Guo, J.P., Li, J., Liu, L., Chen, T.M., Guo, X.R., Lyu, Y.M., Wang, D., Han, Y., Chen, Q., Zhang, Y., 2021. The significant role of radiosonde-measured cloud-base height in the estimation of cloud radiative forcing. Adv. Atmos. Sci. 38 (9), 1552–1565. https://doi.org/10.1007/s00376-021-0431-5.

Yan, Y.F., Liu, Y.M., Lu, J.H., 2016. Cloud vertical structure, precipitation, and cloud radiative effects over Tibetan plateau and its neighboring regions. J. Geophys. Res.-Atmos. 121 (10), 5864–5877. https://doi.org/10.1002/2015jd024591.

Yang, F., Cheng, J., 2020. A framework for estimating cloudy sky surface downward longwave radiation from the derived active and passive cloud property parameters. Remote Sens. Environ. 248, 22. https://doi.org/10.1016/j.rse.2020.111972.

Yang, S., Zou, X., 2013. Temperature profiles and lapse rate climatology in altostratus and nimbostratus clouds derived from GPS RO data. J. Clim. 26 (16), 6000–6014. https://doi.org/10.1175/jcli-d-12-00646.1.

Yang, S., Zou, X., 2017. Lapse rate characteristics in ice clouds inferred from GPS RO and CloudSat observations. Atmos. Res. 197, 105–112. https://doi.org/10.1016/j.atmosres.2017.06.024.

Yang, Y.K., Sun, W.X., Chi, Y.L., Yan, X., Fan, H., Yang, X.C., Ma, Z.S., Wang, Q., Zhao, C.F., 2022. Machine learning-based retrieval of day and night cloud macrophysical parameters over East Asia using Himawari-8 data. Remote Sens. Environ. 273, 19. https://doi.org/10.1016/j.rse.2022.112971.

Yeo, H., Park, S.J., Kim, B.M., Shiobara, M., Kim, S.W., Kwon, H., Kim, J.H., Jeong, J.H., Park, S.S., Choi, T., 2018. The observed relationship of cloud to surface longwave radiation and air temperature at Ny-Ålesund, Svalbard. Tellus B. 70, 10. https://doi.org/10.1080/16000889.2018.1450589.

Zelinka, M.D., Klein, S.A., Hartmann, D.L., 2012. Computing and partitioning cloud feedbacks using cloud property histograms. Part I: cloud radiative kernels. J. Clim. 25 (11), 3715–3735. https://doi.org/10.1175/jcli-d-11-00248.1.

Zhang, J.Q., Chen, H.B., Li, Z.Q., Fan, X.H., Peng, L.A., Yu, Y., Cribb, M., 2010. Analysis of cloud layer structure in Shouxian, China using RS92 radiosonde aided by 95 GHz cloud radar. J. Geophys. Res.-Atmos. 115, 13. https://doi.org/10.1029/2010jd014030.

Zhang, X., Wang, H., Che, H.Z., Tan, S.C., Shi, G.Y., Yao, X.P., 2020. The impact of aerosol on modis cloud detection and property retrieval in seriously polluted East China. Sci. Total Environ. 711, 10. https://doi.org/10.1016/j.scitotenv.2019.134634.

Zhao, C.F., Yang, Y.K., Chi, Y.L., Sun, Y., Zhao, X., Letu, H., Xia, Y., 2023a. Recent progress in cloud physics and associated radiative effects in China from 2016 to 2022. Atmos. Res. 293, 14. https://doi.org/10.1016/j.atmosres.2023.106899.

Zhao, Y., Li, J.M., Zhang, W.Y., Deng, C., Li, Y.R., 2022. Cloud response is significantly biased by CMIP6 over the Tibetan plateau. Geophys. Res. Lett. 49 (17), 11. https://doi.org/10.1029/2022gl100903.

Zhao, Z.J., Zhang, F., Wu, Q., Li, Z.Q., Tong, X., Li, J.W., Han, W., 2023b. Cloud identification and properties retrieval of the Fengyun-4A satellite using a resunet model. IEEE Trans. Geosci. Remote Sens. 61, 18. https://doi.org/10.1109/tgrs.2023.3252023.

Zhu, S.Y., Ma, Z.Q., 2022. Peca-fy4a: precipitation estimation using chromatographic analysis methodology for full-disc multispectral observations from Fengyun-4A/AGRI. Remote Sens. Environ. 282, 22. https://doi.org/10.1016/j.rse.2022.113234.